Comparison of density of states and scattering parameters in coaxial photonic crystals: Theory and experiment

Soufyane Khattou,[1] Madiha Amrani,[1] Abdelkader Mouadili,[2] El Houssaine El Boudouti,[1,*] Abdelkrim Talbi,[3] Abdellatif Akjouj,[4] and Bahram Djafari-Rouhani[4]

[1]*LPMR, Département de Physique, Faculté des Sciences, Université Mohammed I, Oujda, Morocco*

[2]*LPMCER, Département de Physique, Faculté des Sciences et Techniques de Mohammedia, Université Hassan II, Casablanca, Morocco*

[3]*Université de Lille, CNRS, Centrale Lille, ISEN, Université de Valenciennes, UMR 8520 -IEMN - LIA LICS/LEMAC, F-59000 Lille, France*

[4]*IEMN, UMR CNRS 8520, Département de Physique, Université de Lille, 59655 Villeneuve d'Ascq, France*

(Received 16 April 2020; revised 1 October 2020; accepted 6 October 2020; published 21 October 2020)

We present an analytical and experimental study of the scattering parameters in a one dimensional (1D) symmetric photonic crystal and their relation to the density of states (DOS). The 1D photonic crystal is constituted by N alternating wires and loops that are either inserted horizontally or attached vertically between the source and load on a transmission line. The complete knowledge of the scattering matrix coefficients (S_{ij}) allows us to access the DOS and eigenvalues of the finite periodic structure as well as the DOS and dispersion curves of an infinite periodic system. We show the usefulness of the transmission and reflection delay times and highlight their similarities and differences with respect to the DOS, in particular as a function of the absorption strength in the system. For both horizontal and vertical geometries, we show analytically that in a lossless structure, the DOS is proportional to the Friedel phase, namely the derivative of the argument of the determinant of the scattering matrix S. For a low loss system, this proportionality remains still valid with a good approximation and can be used as a practical tool to derive the DOS and therefore the dispersion curves from experimental data. Also, the absorption can be accurately extracted from the measurement of the modulus of the determinant of S. However, for increasing strength of dissipation, we show how and why these relationships cease to be valid. Still, the transmission delay time can remain an efficient tool to derive DOS even at relatively high dissipation strength. Additionally, we show that in the vertical geometry the transmission and reflection delay times exhibit negative delta peaks which are related directly to the eigenmodes of the finite system with different boundary conditions on its extremities. Our theoretical results are obtained by means of the Green's function approach, whereas the experimental demonstrations are performed using standard coaxial cables in the radio-frequency domain.

DOI: 10.1103/PhysRevB.102.165310

I. INTRODUCTION

The concept of density of states (DOS) is of great importance in the calculation of a number of physical quantities such as thermal properties [1] and electron transport in mesoscopic systems [2]. One of the well known methods to calculate the DOS is the Green's function [3–5]. In addition to the DOS, the presence of scatters in a given system is characterized by a scattering matrix which relates the amplitudes of the incoming waves to those of the outgoing waves. The scattering matrix is the main tool used in microwave electrical engineering to understand the response of a system to an incident electromagnetic wave [6]. This quantity is also used in other domains such as transport phenomena in dynamical mesoscopic systems [7], optical switches, and devices [8] as well as quantum mechanics [9]. In the case of one-dimensional (1D) mesoscopic scattering problems, there has been a large number of theoretical studies devoted to understanding the relationship between local and total DOS and different scattering parameters such as the derivative of the phase of the determinant of the scattering matrix S [$\det(S)$] [10–16], the so called Friedel phase [17], and the transmission and reflection delay times [18,19]. The latter studies [18,19] have been performed in order to understand the experiments of Yacoby *et al.* [20] and Schuster *et al.* [21] on quantum dots in the so-called Aharonov-Bohm interferometers [2,22].

In analogy with electron tunneling through a barrier in quantum mechanics [23], several theoretical and experimental works have treated the problem of optical tunneling time, optical clock, Hartmann effect, group delay, and superluminal phenomena [24] in (i) a single layer sandwiched between two media under total internal reflection [25,26], (ii) 1D photonic Bragg reflector (superlattice) made of isotropic and/or anisotropic layers [27–31], (iii) microwave waveguide under cutoff frequency or with a birefringent Fabry-Perot cavity [32–34], (iv) optical fiber at the cutoff wavelength [35], (v) metamaterials and microresonators [36,37], and (vi) coaxial photonic crystals [38–42]. (vii) Also, a large amount of work has been performed on electromagnetic periodic structures called frequency selective surface (FSS)[43]. Diverse FSS structures have been designed in different domains ranging

*Corresponding author: elboudouti@yahoo.fr

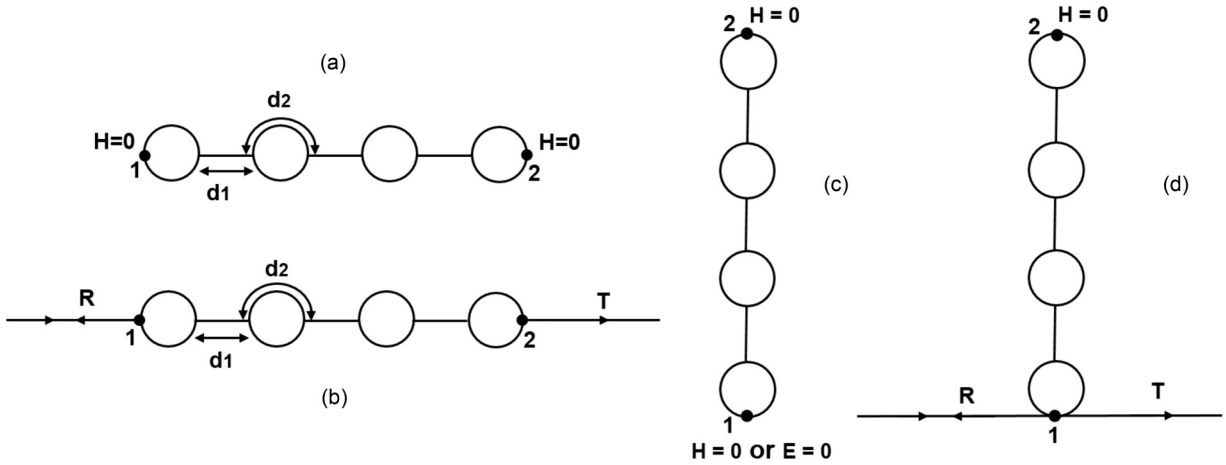

FIG. 1. (a) Schematic representation of the finite periodic structure made of $N = 4$ cells with $H = 0$ boundary condition on both sides. Each cell is composed of a wire of length d_1 and a loop formed out by two wires, each of length d_2. (b) The finite periodic structure inserted between two semi infinite wires. (c) The finite structure with $H = 0$ boundary condition on one side and $H = 0$ or $E = 0$ on the other side. (d) The finite periodic structure grafted vertically on a waveguide.

from microwave to optical regime with a variety of applications such as: antenna filter, microwave absorbing, sensors, textile... In addition, the theoretical analysis of the DOS has been performed in dielectric [44,45], plasma [46], and metamaterial layered media [47]. From the experimental point of view, the DOS is generally extracted from measurable quantities related to DOS such as: the differential conductance in scanning tunneling spectroscopy to deduce electron charge density [48], the conductivity correction due to electron-electron interaction in semiconductors to derive the Fermi's energy [49] and the nuclear resonant scattering to obtain the phonon DOS [50]. To our knowledge, little works have been performed to compare both analytically and experimentally the calculated DOS and different experimental scattering parameters in photonic crystals [51,52]. Also, in most of the theoretical demonstrations, the systems are supposed lossless [44,45] which hidden interesting information related to the existence of transmission and reflection zeros. Some years ago [51,52], we have given a comparative study of the DOS and the derivative of the phase of the scattering matrix as well as the transmission delay time in a double stub lossy structure inserted along a waveguide and supporting Fano and induced transparency resonances. Such a study requires simple analytical calculation and experimental equipment, but enables deep understanding of all these phenomena.

In this paper, we present an analytical and experimental comparative study of DOS and scattering parameters in a finite 1D coaxial photonic crystal made of N cells attached either horizontally or vertically along a waveguide (see Fig. 1). In particular, (i) we demonstrate analytically that in a lossless system, the DOS is proportional to the derivative of the argument of $\det(S)$, the so-called Friedel phase [17]. Then we show that this proportionality remains valid with a good approximation for relatively low loss systems, which enables to determine experimentally the DOS and therefore the dispersion curves. (ii) We show that the absorption can be extracted from the modulus of the determinant of S. However, for high loss systems, we show that contrary to the theoretical demonstrations established before for lossless or low loss mesoscopic systems, all these relations are no longer valid and the DOS can be derived only from the transmission delay time in the horizontal structure. (iii) We highlight that the DOS may exhibit a different behavior in comparison with reflection delay time. In a lossless structure, this difference only comes from negative delta peaks in the delay times which actually contain useful information about the eigenvalues of our finite scattering system. In a lossy structure, the latter delta peaks become broadened (anti-resonances) and hence observable in the experimental measurements. Using the Green's function method [5,53], we derive exact analytical expressions relating the DOS and different scattering parameters for a symmetric photonic crystal made of periodic repetition of wires and loops. This structure can be grafted either horizontally or vertically between two semi-infinite waveguides. Also, in the case of the vertical structure, we demonstrate that the negative delta peaks associated to the transmission delay time give the eigenmodes of the system with $H = 0$ boundary condition on one side and $E = 0$ on the other side. However, the negative delta peaks associated to the reflection delay time give the eigenmodes of the finite structure with $H = 0$ boundary condition on both sides, H and E being the magnetic and electric fields respectively. Finally, we show that both (horizontal and vertical) structures give almost similar results as concerns the DOS of the system, however, the vertical structure is rich of information as it enables to extract also the confined and surface modes of the photonic crystal with different boundary conditions on its extremities. The experiments are carried out using coaxial cables in the radio-frequency regime. It is worth mentioning that 1D system like coaxial cables have been shown to be good candidates for highlighting general rules about confined and surface electromagnetic modes in finite size 1D structures [54]. Also, it was shown that coaxial cables present an easily realizable experimental approach to the study of wave interference phenomena such as band gap structures with or without defect modes [42,55,56], superluminal and subluminal effects [51,52], and quasicrystals [57,58].

The rest of the paper is organized as follows. In Sec. II, we give the calculation method used in this work which is based

on the interface response theory of continuous media [5,53]. We derive the Green's function of the finite structure and the dispersion relation of the infinite photonic crystal (Fig. 1). Also, we describe briefly the experimental setup used in this study. In Sec. III, we present an analytical and experimental comparative study of DOS and scattering matrix S parameters, namely its argument and modulus, for the finite size photonic structure attached horizontally along a waveguide [Fig. 1(b)]. Also, we discuss both theoretically and experimentally the expressions relating the DOS and the reflection and transmission delay times. In Sec. IV, we give the same study as in Sec. III but for the vertical structure [Fig. 1(d)]. The conclusion is presented in Sec. V.

II. GREEN'S FUNCTION APPROACH AND EXPERIMENTAL SETUP

The theoretical method is performed using the interface response theory of continuous media [5,53], which enables the calculation of the Green's function of any heterogeneous material with different interfaces and then densities of states as well as transmission and reflection coefficients. In what follows, we shall avoid the details of this calculation which are given in Appendices A and B and give only the necessary Green's function elements of the structure studied here that enables to deduce the DOS and the scattering matrix elements, namely the transmission and reflection coefficients. We consider a finite 1D coaxial photonic crystal made of N cells with $H = 0$ boundary conditions on both sides [Fig. 1(a)]. Each cell is composed of a wire of length d_1 and impedance Z and a loop formed out by two wires, each of length d_2 and impedance Z. The loop is equivalent to a wire of length d_2 and impedance $Z/2$. Therefore the photonic crystal becomes equivalent to a Bragg reflector made of two wires characterized by two different lengths d_1 and d_2 and two different impedances Z and Z/2 respectively and $d = d_1 + d_2$ is the period of the structure.

The dispersion relations of the infinite and finite photonic crystals made of a wire and a loop require first the knowledge of the inverse of the Green's functions of these elementary constituents (see Appendix A). In all the expressions, will appear the following basic parameters of the wires and the loops, namely, the parameters $a = -jF\frac{C_1}{S_1}$ and $b = jF\frac{1}{S_1}$ of the wire and $A = -j2F\frac{C_2}{S_2}$ and $B = j2F\frac{1}{S_2}$ of the loop where $C_i = \cos(kd_i)$, $S_i = j\sin(kd_i)$ $(i = 1$ and $2)$ and $j = \sqrt{-1}$. $k = \frac{\omega}{c}\sqrt{\varepsilon}$ is the wave number, which is directed along the direction of the wire and $F = \frac{\omega}{Z}$. ε and Z are the permittivity and the impedance of the waveguides, respectively.

From the above parameters, one can deduce the dispersion relation of the infinite photonic crystal (see Appendix A), namely,

$$\cos(k_B d) = \cos(kd_1)\cos(kd_2) - \tfrac{5}{4}\sin(kd_1)\sin(kd_2). \quad (1)$$

where k_B is the Bloch wave number of the infinite photonic crystal.

Using the Green's function method [53], the inverse of the Green's function $g_0^{-1}(M, M)$ of the photonic crystal made of N cells, in the space of interface $M = \{1, 2\}$ at its two extremities labeled 1 and 2 [Fig. 1(a)], can be obtained in a compact form (see Appendix A for the details of calculation),

$$g_0^{-1}(M, M) = \begin{pmatrix} A_N & B_N \\ B_N & A_N \end{pmatrix} \quad (2)$$

where the expressions of A_N and B_N are given by

$$A_N = \frac{Y_1}{\Delta(A+a)}\Big[\Delta - Bb\Big(t - \frac{1}{t}\Big)Y_1\Big] \quad (3a)$$

and

$$B_N = Bb\Big(t - \frac{1}{t}\Big)\frac{Y_1 Y_2}{(A+a)\Delta}t^{(N-1)}. \quad (3b)$$

The expressions of Y_1, Y_2 and Δ are given by

$$Y_1 = b^2 - a^2 - aA + Bbt,\ Y_2 = aB - Abt,\ \text{and}$$
$$\Delta = Y_1^2 - Y_2^2 t^{2(N-1)}, \quad (4)$$

where the parameter t is defined as $t = e^{jk_B d}$.

The eigenmodes of the photonic crystal with $H = 0$ boundary conditions on both sides [Fig. 1(a)] are given by (see Appendix A)

$$det\big[g_0^{-1}(M, M)\big] = A_N^2 - B_N^2 = 0. \quad (5)$$

From Eqs. (3a) and (3b), one can write $A_N^2 - B_N^2$ in the following explicit form:

$$A_N^2 - B_N^2 = \Big(\frac{Y_1}{A+a}\Big)^2 \frac{1}{\Delta}\Big[Y_1 - Y_2 t^{N-1} - Bb\Big(t - \frac{1}{t}\Big)\Big] \times \Big[Y_1 + Y_2 t^{N-1} - Bb\Big(t - \frac{1}{t}\Big)\Big], \quad (6)$$

where the terms between brackets in Eq. (6) give the symmetric and antisymmetric modes. In a similar way, one can show that the eigenmodes of the finite photonic crystal with $E = 0$ boundary conditions on both sides are given by

$$\Delta = [Y_1 - Y_2 t^{(N-1)}][Y_1 + Y_2 t^{(N-1)}] = 0. \quad (7)$$

This quantity Δ appears in the denominators of A_N [Eq. (3a)], B_N [Eq. (3b)], and $A_N^2 - B_N^2$ [Eq. (6)] and hence its zeros correspond to the poles of all these functions. Here also, the terms between brackets in Eq. (7) give the symmetric and antisymmetric modes.

Similarly, the eigenmodes of the finite structure with $E = 0$ boundary condition on its bottom side and $H = 0$ on its top side [Fig. 1(c)] are given by (see Appendix A)

$$A_N = 0. \quad (8)$$

The experimental results are performed using standard coaxial cables RG-58/U connected by standard BNC-T connectors. The cables are characterized by the complex permittivity $\varepsilon = 2.3 + j\varepsilon''$ and the impedance $Z = 50\Omega$. The lengths of the cables are $d_1 = d_2 = 1m$ and the period $d = d_1 + d_2 = 2m$. The dissipation in the cables is considered through the imaginary part of ε which is frequency dependent [42,51]. The scattering matrix S of the 1D photonic crystal was measured in the frequency range 1-200 MHz by means of a broadband vector network analyzer Agilent PNA-X N5242A. The details of the experimental setup is given in Appendix B.

III. HORIZONTAL STRUCTURE: ANALYTICAL AND EXPERIMENTAL RESULTS

In this section, we give an analytical and experimental comparative study of DOS and scattering parameters, namely the phase and modulus of the scattering matrix and of transmission and reflection coefficients, for a finite size photonic crystal attached horizontally along a waveguide [Fig. 1(b)]. First, we show analytically that for lossless structure (i.e., $\varepsilon'' = 0$), the DOS is proportional to the derivative of the phase of $\det(S_h)$, the so-called Friedel phase [17] (the subscript h refers to the horizontal structure). Then we show that this proportionality remains valid with a very good approximation for relatively low loss systems, which enables to extract experimentally the DOS from the scattering matrix S_h and therefore the dispersion curves. Also, the absorption coefficient can be extracted from the modulus of $\det(S_h)$. However, for high loss systems, these relations are no longer valid. In addition, we discuss the relation between the DOS and the reflection and transmission delay times. Contrary to the derivative of the phase of $\det(S_h)$, we show that the transmission delay time represent very well the DOS even in presence of loss and remains robust for high loss systems. However, the reflection delay time is different from the DOS because of the negative delta peaks due to the reflection zeros. The finite 1D photonic crystal is made of N cells [Fig. 1(a)]. Each cell is composed of a wire of length $d_1 = 1m$ and a loop formed out by two wires, each of length $d_2 = 1m$, $d = d_1 + d_2 = 2m$ is the period of the photonic crystal. The symmetric loop is simply two lines in parallel, each has a length $d_2 = d_1$ and an impedance Z. The loop circuit can be considered equivalent to a wire of length d_2 and impedance $Z/2$. Therefore the periodic structure in Fig. 1 is equivalent to alternating two cables with different impedances Z and $Z/2$. This choice enables to create a large impedance mismatch between the two elements, which enables to get large band gaps [42,54].

A. Density of states and scattering phase

The inverse of the Green's function of the whole structure depicted in Fig. 1(b) in the space of interface $M = \{1, 2\}$ at its both extremities, is given by

$$g_h^{-1}(M, M) = \begin{pmatrix} A_N - jF & B_N \\ B_N & A_N - jF \end{pmatrix} \tag{9}$$

where $-jF$ is the inverse Green's function of the semi-infinite wires surrounding the finite system with $F = \frac{\omega}{Z}$.

The expressions of transmission and reflection coefficients for the horizontal structure depicted in Fig. 1(b) are given, respectively, by Ref. [53] (see Appendix C for the details of calculation)

$$t_h = 2jFB_N \det[g_h(M, M)] \tag{10a}$$

and

$$r_h = -C_N \det[g_h(M, M)], \tag{10b}$$

where $\det[g_h(M, M)]$ and C_N are given respectively by

$$\det[g_h(M, M)] = \frac{1}{A_N^2 - B_N^2 - F^2 - 2jFA_N} \tag{11}$$

and

$$\begin{aligned} C_N &= A_N^2 - B_N^2 + F^2 \\ &= j2\left(A_1^2 - B_1^2 + F^2\right)\left(Y_1^2 - Y_2^2\right)t^{N-2}\sin(Nk_Bd). \end{aligned} \tag{12}$$

Another interesting quantity that enables to deduce the distribution and the weight of the different modes in the system is the DOS of the whole structure. However, as the system is composed of a finite-size photonic crystal inserted between two semi-infinite waveguides, we need to calculate the variation of the DOS ($\Delta n_T(\omega)$) between the system in Fig. 1(b) and a reference system to avoid any divergency in DOS due to the semi-infinite wires. This quantity can be calculated by integrating the local DOS over the whole system and to subtract the density of states of the infinite waveguide such as [59]

$$\Delta n_T(\omega^2) = n_1(\omega^2) + 2n_2(\omega^2) + 2\Delta n_s(\omega^2), \tag{13}$$

where $n_1(\omega^2)$ and $n_2(\omega^2)$ are the contributions of wires 1 and 2 of the photonic crystal, respectively, and $\Delta n_s(\omega^2)$ comes from the two semi-infinite waveguides surrounding the photonic crystal. These three quantities are given explicitly in Appendix F.

In order to give an analytical comparison of the DOS with the scattering parameters (see below), there exists another way to get a compact expression of the variation of the DOS. This method consists to consider the variation of the DOS $\Delta n_h'(\omega)$ for the structure in Fig. 1(b) and a reference system formed out of the same volumes of the decoupled semi-infinite wires and the finite structure [Fig. 1(a)]. In this case, $\Delta n_h'(\omega)$ can be obtained from the following equation [60]:

$$\Delta n_h'(\omega) = \frac{1}{\pi}\frac{d}{d\omega}\mathrm{Arg}\left\{\det\left[\frac{g_h(M, M)}{g_0(M, M)F^{-2}}\right]\right\}. \tag{14}$$

Now, if we subtract the eigenmodes of the finite structure with $H = 0$ boundary conditions on both sides [Eqs. (A27) and (6)], Eq. (14) becomes simply

$$\Delta n_h(\omega) = \frac{1}{\pi}\frac{d}{d\omega}\mathrm{Arg}\{\det[g_h(M, M)]\}. \tag{15}$$

Equations (13) and (15) are similar, however Eq. (15) should be handled carefully in order avoid the eigenmodes of the finite structure which appear as delta functions in $\det[g_h(M, M)]$ [Eqs. (3a), (3b), (6), and (11)]. Whereas Eq. (13) is more interesting as it does not contain such useless delta functions associated with the reference system.

Another important quantity which gives us more information about the scattering parameters of the system such as reflection and transmission coefficients as well as the Friedel phase [17], is the scattering matrix S_h. For the symmetric horizontal system, S_h is defined by

$$S_h = \begin{pmatrix} r_h & t_h \\ t_h & r_h \end{pmatrix}, \tag{16}$$

where r_h and t_h are the reflection and transmission coefficients given by Eqs. (10a) and (10b), respectively.

Now, we shall give first exact analytical relations between the DOS and the scattering phase for lossless media and then we shall see numerically and experimentally the effect of the presence of loss on such relationship. Indeed, in the absence

of loss (i.e., $\varepsilon'' = 0$), A_N and B_N [Eqs. (3a) and (3b)] are real quantities, therefore, we can check easily (see Appendix C) that the transmission and reflection rates $T_h = |t_h|^2$ and $R_h = |r_h|^2$ verify the conservation energy $T_h + R_h = 1$. In addition, the phase of the determinant of the scattering matrix S_h [Eq. (16)] can be deduced from the expressions of r_h and t_h [Eqs. (10a) and (10b)] (see Appendix D), namely,

$$\frac{d}{d\omega}\text{Arg}[\det(S_h)] = \frac{d}{d\omega}\text{Arg}\left[r_h^2 - t_h^2\right] = 2\frac{d}{d\omega}\text{Arg}\{\det[g_h(M,M)]\}. \quad (17)$$

From Eqs. (15) and (17), one can deduce that the DOS is related to the phase of the determinant of the scattering matrix such as

$$\frac{1}{2}\frac{d}{d\omega}\text{Arg}[\det(S_h)] = \pi\,\Delta n_h(\omega). \quad (18)$$

It is worth noticing that the Friedel phase is defined as the cumulative phase of the eigenvalues of the scattering matrix [17], this quantity is simply the phase of the determinant of the scattering matrix (see Ref. [61] for the derivative of this relation in 1D graphs). Equation (18) clearly shows that the DOS can be extracted from the measurement of the phase of $\det(S_h)$, the so-called Friedel phase [17,61]. Also, in absence of loss, we can check easily the well known relation $|\det(S_h)| = R_h + T_h = 1$ (see Appendix E).

For low loss systems, we have checked numerically and experimentally that Eqs. (17) and (18) still remain valid with a good approximation (see below). In addition, the absorption can be derived from $|\det(S_h)|$ through the relation [62]

$$A_h \simeq 1 - |\det(S_h)|. \quad (19)$$

However, for high loss systems, all the above results [Eqs. (17)–(19)] are no longer valid, nevertheless the DOS can be extracted from the transmission delay time (see below).

Figure 2(a) gives the band gap structure for an infinite photonic crystal (black curves) made of alternating segments and loops made of standard coaxial cables ($Z = 50\ \Omega$) of lengths $d_1 = d_2 = 1m$. In this case, the dispersion relation [Eq. (1)] reduces to

$$\cos(k_B d) = 1 - \tfrac{9}{4}\sin^2(kd_1). \quad (20)$$

The segments and loops play the role of quarter wavelength layers at the dimensionless frequencies $kd_1 = \omega d_1\sqrt{\varepsilon}/c = (2n+1)\pi/2$ (n is an integer). In absence of loss, these frequencies correspond also to mid-gaps around $f =$ 49 MHz, 147 MHz, … Also, the band-gap edges are given by $\cos(k_B d) = \pm 1$ [Eq. (20)]. The band edges at the center of the Brillouin zone [i.e., $\cos(k_B d) = 1$] are given by $kd_1 = 0, \pi, 2\pi, \ldots$ (i.e., $f = 0$, 98 MHz, 196 MHz, …). For these frequencies, the gaps close [Fig. 2(a)], this is a characteristic of quarter wavelength layers. However, the band edges at the limit of the Brillouin zone [i.e., $\cos(k_B d) = -1$] are given by $\sin(kd_1) = \pm 2\sqrt{2}/3$ (i.e., $f = 38$ MHz, 60 MHz, 137 MHz, 158 MHz,...). These values are in accordance with the numerical results in Fig. 2(a). Open circles in Fig. 2(a) give the experimental dispersion curves obtained from the scattering matrix as explained below.

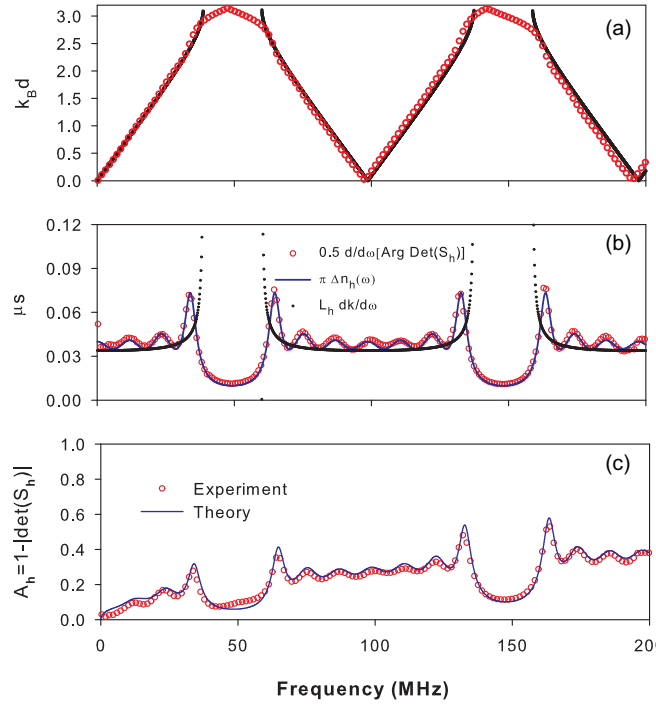

FIG. 2. (a) Theoretical band gap structure of an infinite structure made of segments and loops as shown in Fig. 1 (i.e., N = 4 cells). Open circles give the experimental results extracted from the scattering matrix. (b) Variation of $\frac{1}{2}\frac{d}{d\omega}\text{Arg}[\det(S_h)]$ (in units of μs) obtained from the scattering matrix S_h (open circles), and the variation of DOS ($\Delta n_h(\omega)$) obtained from [Eq. (15)] (solid line). Dotted line shows the variation of DOS derived from the theoretical dispersion curves of the infinite system in (a). (c) Variation of the absorption coefficient (open circles) derived from $\det(S_h)$ [Eq. (19)] in comparison with the theoretical results (solid lines).

Figure 2(b) shows half of the derivative of the experimental phase of $\det(S_h)$ as function of frequency (open circles), and the calculated variation of DOS (solid line) obtained from Eq. (15) [or equivalently Eq. (13)]. One can notice a very good agreement between $\pi\,\Delta n_h(\omega)$ and $\frac{1}{2}\frac{d}{d\omega}\text{Arg}[\det(S_h)]$ in accordance with Eq. (18). These results give an experimental measurement of the DOS of the horizontal photonic crystal [Fig. 1(b)]. Also, despite the small number of cells, the DOS exhibits the same behavior that the DOS derived from the dispersion curves (dotted line) of the infinite periodic structure depicted in Fig. 2(b) and obtained from the relation [63]

$$\Delta n_h(\omega) = \frac{L_h}{\pi}\frac{dk}{d\omega}, \quad (21)$$

where L_h is the effective length of the finite structure ($L_h \simeq$ 7 m). As predicted, the DOS of the infinite system diverges at the edges of the band gaps which is a well known property of the 1D systems [63], whereas the DOS of the finite system (solid line) exhibits small oscillations inside the allowed bands. The number of oscillations is related to the number of periods in the finite system. Conversely, from the integration of the experimental DOS in Fig. 2(b), we can reproduce the dispersion curves in Fig. 2(a) (open circles) using Eq. (21). Despite the small number of loops ($N = 4$) for the finite structure, the dispersion curves obtained from the scattering

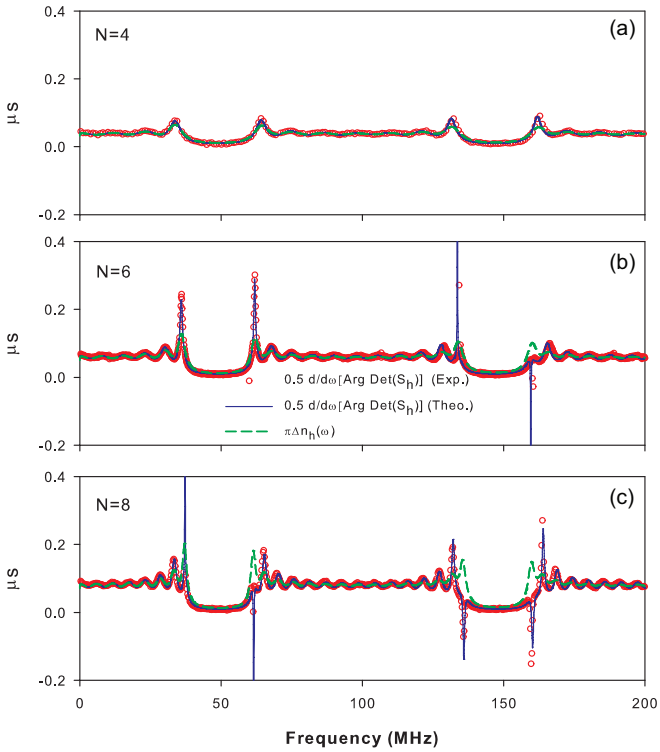

FIG. 3. (Blue solid line) Theoretical variation of half of the derivative of the argument of $\det(S_h)$ ($\frac{1}{2}\frac{d}{d\omega}\mathrm{Arg}[\det(S_h)]$), and the variation of DOS ($\Delta n_h(\omega)$) obtained from [Eq. (15)] (green dashed line) for different values of the number of cells N. Red open circles give the experimental results of $\frac{1}{2}\frac{d}{d\omega}\mathrm{Arg}[\det(S_h)]$ obtained from the scattering matrix S_h data.

matrix, describe very well the band structure for the infinite structure ($N \to \infty$) [red circles in Fig. 2(a)].

Figure 2(c) presents the absorption coefficient derived from the modulus of $\det(S_h)$ [Eq. (19)]. This result shows that in presence of low loss, one can easily derive the amplitude of absorption from the measurements of complex reflection and transmission coefficients and hence $\det(S_h)$. As predicted, the absorption in the bands [Fig. 2(c)] increases almost linearly with the frequency, whereas it presents dips in the gap regions where the waves are mostly reflected. The experimental results (open circles) are in very good agreement with the theoretical ones (solid lines).

As mentioned above, the relation between the DOS and the derivative of the argument of $\det(S_h)$ [Eq. (18)] as well as the relation between the absorption and $|\det(S_h)|$ [Eq. (19)] are exact for lossless media. However, the numerical and experimental results in Fig. 2 show that these relations remain valid with a good approximation in relatively low loss system. The presence of loss can affect considerably the above relations, this quantity which is responsible of the decreasing of the amplitude of waves, occurs through the attenuation coefficient. The latter quantity arise either through the imaginary part of the permittivity or the increase in the length of the structure. In order to give a better insight about the effect of high loss on these relations, we have plotted in Figs. 3(a)–3(c) a comparison between DOS and $\frac{1}{2}\frac{d}{d\omega}\mathrm{Arg}[(\det(S_h)]$ for different values of the number of cells N. We clearly see that the DOS is approximately equivalent to the derivative of the phase of $\det(S_h)$ for $N = 4$ [Fig. 3(a)]. We can see that the DOS remains almost the same as the derivative of the phase of $\det(S_h)$ inside the bands with a noticeable discrepancy between the two spectra at the bulk band edges. Also, we have checked numerically that the total number of modes [obtained from the integral of DOS or the derivative of the phase of $\det(S_h)$] give almost the same results. However, for $N > 4$ [Figs. 3(b) and 3(c)], the DOS and the derivative of the phase of $\det(S_h)$ exhibit different behaviors especially at the band edge frequencies where the latter changes sign. Indeed, we have checked that $\det(S_h)$ vanishes at these frequencies (i.e., $r = \pm t$) and changes sign, giving rise to an abrupt phase change of π in the argument of $\det(S_h)$ and therefore a negative delta peak in the derivative of the phase of $\det(S_h)$. These results are displayed in Figs. 3(b) and 3(c). The theoretical results of $\frac{1}{2}\frac{d}{d\omega}\mathrm{Arg}[(\det(S_h)]$ are confirmed experimentally by red open circles in Figs. 3(a)–3(c). We can see that for $N > 4$, the DOS displayed by green dashed curves show a different behavior than $\frac{1}{2}\frac{d}{d\omega}\mathrm{Arg}[(\det(S_h)]$ especially at the band edges where $\det(S_h)$ changes sign. Figure 4 gives a comparison between the absorption $A_h = 1 - R_h - T_h$ (left panel) and $1 - |(\det(S_h)|$ (right panel) for different values of the number of cells N. We can see a discrepancy between the two latter quantities as far as N increases [see Figs. 4(b), 4(e) and 4(c), 4(f)]. In particular, at the band edges when $\det(S_h)$ almost vanishes, the absorption becomes simply $A_h = 1 - 2R_h$ (as $R_h = T_h$) whereas $1 - |(\det(S_h)|$ becomes almost unity (as $\det(S_h) = 0$). The theoretical results of $A_h = 1 - R_h - T_h$ and $1 - |(\det(S_h)|$ are confirmed experimentally by red open circles in Figs. 4(a)–4(f). As mentioned above, the effect of loss can be also analyzed through an analysis of the imaginary part of the permittivity (i.e., ε'') for a fixed number of cells N. These results are displayed in Appendix G.

B. Density of states and delay times

In order to derive exact relations between DOS and delay times, we shall first consider the case of lossless media. Indeed, from Eq. (10a), one can obtain the transmission delay time which is defined as the derivative of the corresponding phase versus the pulsation ω, namely,

$$\tau_T^h = \frac{d\theta_T^h}{d\omega} = \frac{d}{d\omega}\mathrm{Arg}\{\det[g_h(M,M)]\} + \pi \sum_n \left[\mathrm{sgn}\frac{dB_N}{d\omega}|_{\omega=\omega_n}\right]\delta(\omega-\omega_n). \quad (22)$$

By the same way, the reflection delay time τ_R^h can also be derived from Eq. (10b) as

$$\tau_R^h = \frac{d\theta_R^h}{d\omega} = \frac{d}{d\omega}\mathrm{Arg}\{\det[g_h(M,M)]\} + \pi \sum_n \left[\mathrm{sgn}\frac{dC_N}{d\omega}|_{\omega=\omega_n}\right]\delta(\omega-\omega_n) \quad (23)$$

θ_T^h and θ_R^h are the phases of the transmission and reflection coefficients respectively. *sgn* means the sign function and ω_n represents the frequencies where the expressions B_N and C_N

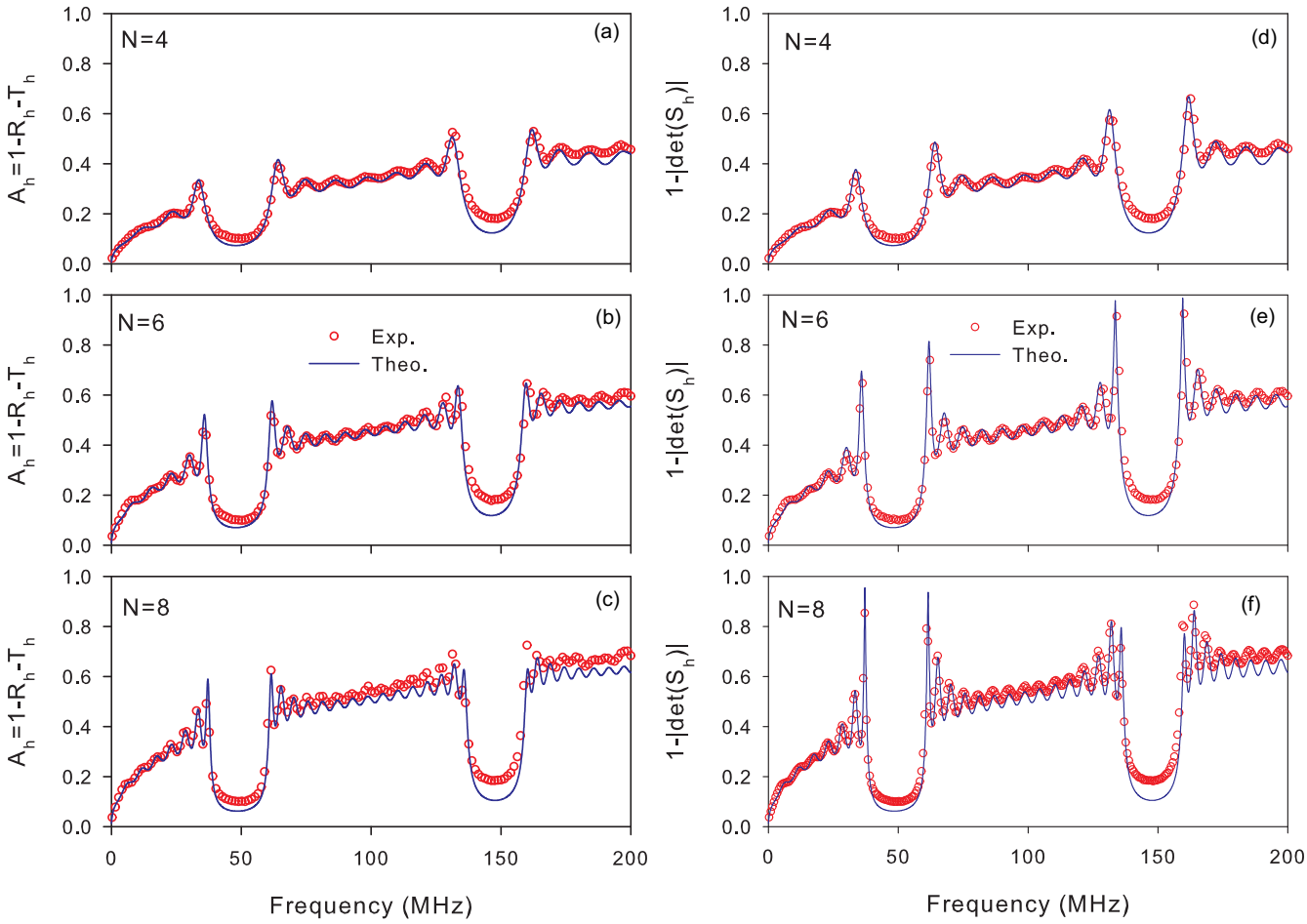

FIG. 4. Comparison between the absorption $A_h = 1 - R_h - T_h$ (left panel) and $1 - |(\det(S_h)|$ (right panel) for different values of the number of cells N. Blue lines (red open circles) give the theoretical (experimental) results.

change sign, and the corresponding phases exhibit a jump of π.

The horizontal structure does not give any transmission zero as $B_N \neq 0$ [Eq. (10a)], then $\mathrm{Arg}(B_N) = 0$ or π and therefore from Eqs. (15) and (22) one can deduce that

$$\tau_T^h = \pi \Delta n_h(\omega). \tag{24}$$

However, Eqs. (15) and (23) show that τ_R^h is different from $\Delta n_h(\omega)$, as C_N [Eq. (12)] can vanish for $N-1$ frequencies in each band given by the following Bloch wave number

$$k_B = m\pi/Nd, m = 1, 2, \ldots, N-1, \tag{25}$$

and the corresponding phase of C_N exhibits a jump of π. Therefore the reflection delay time presents negative delta peaks and one deduces that

$$\tau_R^h \neq \pi \Delta n_h(\omega). \tag{26}$$

Equations (15) and (23) show that for lossless media, apart from the existence of delta peaks in τ_R^h, this latter quantity is equivalent to DOS. However, in presence of loss, the above Eqs. (22) and (23) remain valid. In addition, because of loss, the true delta functions in the reflection delay time [Eq. (23)] broaden and become antiresonances (with a Lorentzian shape), which enables their easy observation in the experiments (see below).

Figure 5(a) reproduces the band structure of the infinite system [Fig. 2(a)] made of alternating segments and loops made of standard coaxial cables ($Z = 50\ \Omega$) of lengths $d_1 = d_2 = 1m$. Figure 5(b) shows the transmission amplitude for a finite structure made of N = 4 loops. Despite the small number of cells, the positions of the gaps (transmission dips) coincide clearly with those of the infinite system. Increasing the number of cells will affect considerably the amplitude of the transmission [Fig. 5(b)] because of the loss effect in the cables, whereas the overall results such as gap widths and dispersion curves [Fig. 2(a)] remain almost unaffected. Figures 5(c) and 5(d) give the transmission phase and the corresponding delay time. One can see that the phase increases monotonically, and the delay time reflects the DOS inside the finite structure as described in Fig. 5(e). One can notice that the DOS is directly proportional to the transmission delay time in accordance with Eq. (24). The experimental results (open circles) are in very good agreement with theory (solid lines).

Figure 6 illustrates the same results as in Figs. 5(b)–5(d), but for the reflection coefficient. One can notice that the amplitude of the reflection vanishes $N-1$ times in each band [Eq. (25)], giving rise to N-1 phase drops [Fig. 6(b)] and therefore $N-1$ negative delay times [Fig. 6(c)], which do not exist in the DOS [Fig. 5(e)]. These results show that, contrary to the transmission delay time, the reflection delay time is different

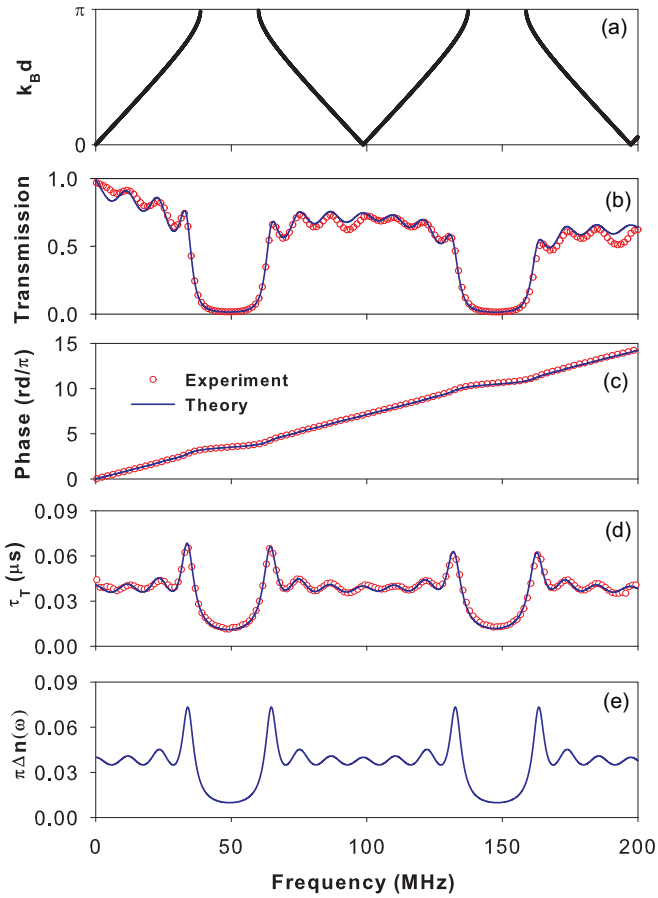

FIG. 5. (a) Theoretical band gap structure of an infinite structure made of segments and loops as shown in Fig. 1. (b) Transmission amplitude through the finite size system composed of N = 4 cells [Fig. 1(b)]. [(c) and (d)] Transmission phase and the corresponding delay time. (e) DOS of the finite structure in Fig. 1(b). Open circles show the experimental results, whereas solid lines correspond to the theoretical ones.

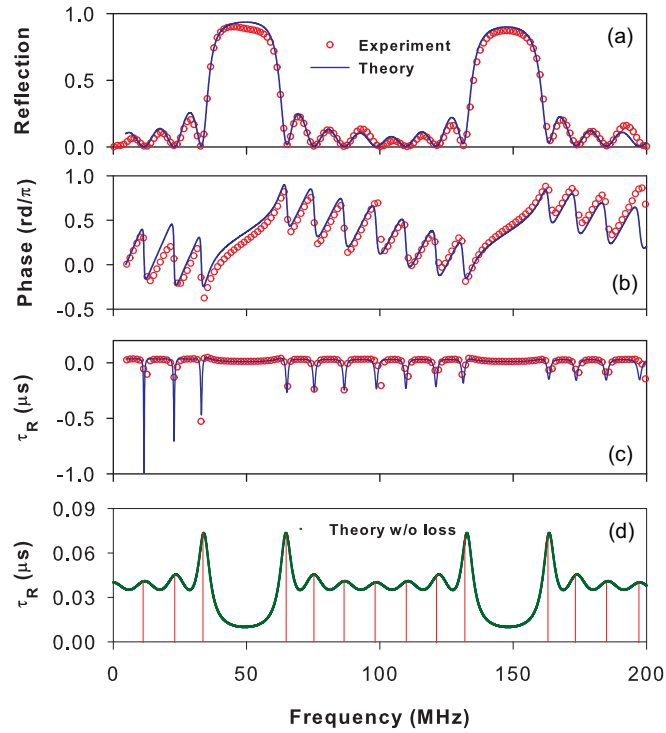

FIG. 6. (a) Reflection amplitude through the finite size system composed of N = 4 cells [Fig. 1(b)]. [(b) and (c)] Reflection phase and the corresponding delay time. Open circles show the experimental results, whereas solid lines correspond to the theoretical ones. (d) Reflection delay time in absence of loss, the vertical bars indicate the positions of delta peaks. It is worth noticing that (c) and (d) are not plotted with the same scale.

from the DOS in accordance with Eq. (26). The delta peaks in Fig. 6(c) are broadened because of the existence of the dissipation in the cables. The experimental results (open circles) are in very good agreement with theory (solid lines). Let us mention that negative delta peaks in the reflection spectra have been provided experimentally on microstrip dielectric slabs and Bragg reflectors [64] with particular interest in superluminal phenomenon [40,41]. In the absence of dissipation, the reflection and transmission delay times seems equivalent [45] as the negative peaks now become true delta peaks invisible in the reflection delay time spectra. To give a better insight, the behavior of the theoretical reflection delay time versus the frequency in absence of dissipation is plotted in Fig. 6(d). We can see clearly that, apart the true delta peaks indicated by vertical bars, the reflection delay time is proportional to the transmission delay time [Fig. 5(d)] and to the DOS [Fig. 5(e)]. However, in presence of loss, the transmission and reflection delay times for a symmetric structure [Figs. 5(d) and 6(c)] are not equivalent because of the additional negative delta peaks [Eq. (23)] induced by the term $C_N = 0$ [Eq. (12)]. In order to show clearly the effect of loss on the relation between DOS and reflection delay time in presence of reflection zeros, we have plotted in Appendix H (see Fig. 14), the theoretical reflection coefficient and the corresponding delay times for different values of loss.

In order to give a better insight about the behavior of transmission and reflection delay times for high loss systems, we have presented in Figs. 7 and 8, respectively, a comparison between DOS, transmission and reflection delay times for different values of the number of cells N. Red open circles give the experimental results. Contrary to the derivative of the phase of $\det(S_h)$, the transmission delay time in Fig. 7 represents very well the DOS even in presence of loss and remains robust even for high loss systems [Figs. 7(b) and 7(c)]. Figures 8(a)–8(c) show a comparison between DOS and reflection delay time for different values of N. We can see that according to Eq. (26) the reflection delay time is different from the DOS (green curves in Fig. 8) because of the existence of negative delta peaks due to reflection zeros giving by Eq. (12) for $N-1$ frequencies in each band. The main difference consists in the possibility of observing true delta peaks (with zero width) in the reflection delay time which become broadened due to dissipation in the cables. Even though the negative delta peaks in the delay time damage drastically the shape of the DOS, the existence of such negative peaks represent a practical tool to deduce directly the frequency positions of the confined and surface modes of a finite photonic crystal with different boundary conditions on

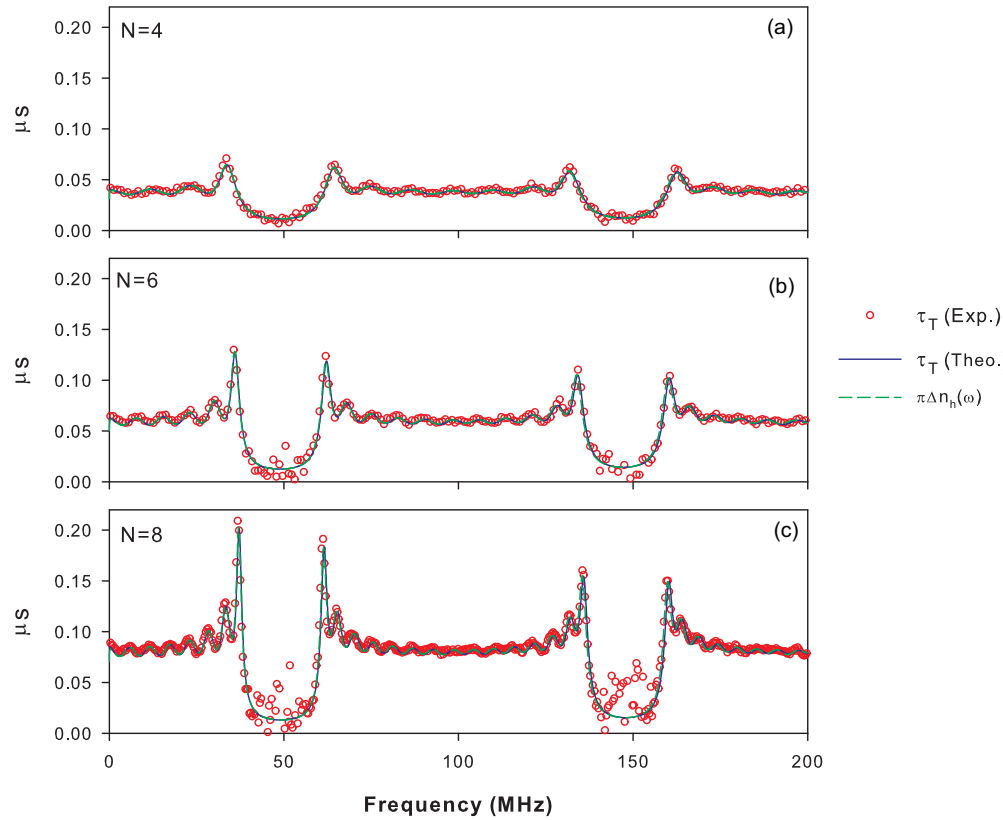

FIG. 7. Comparison between DOS and transmission delay time for different values of N. Open circles give the experimental results of transmission delay time.

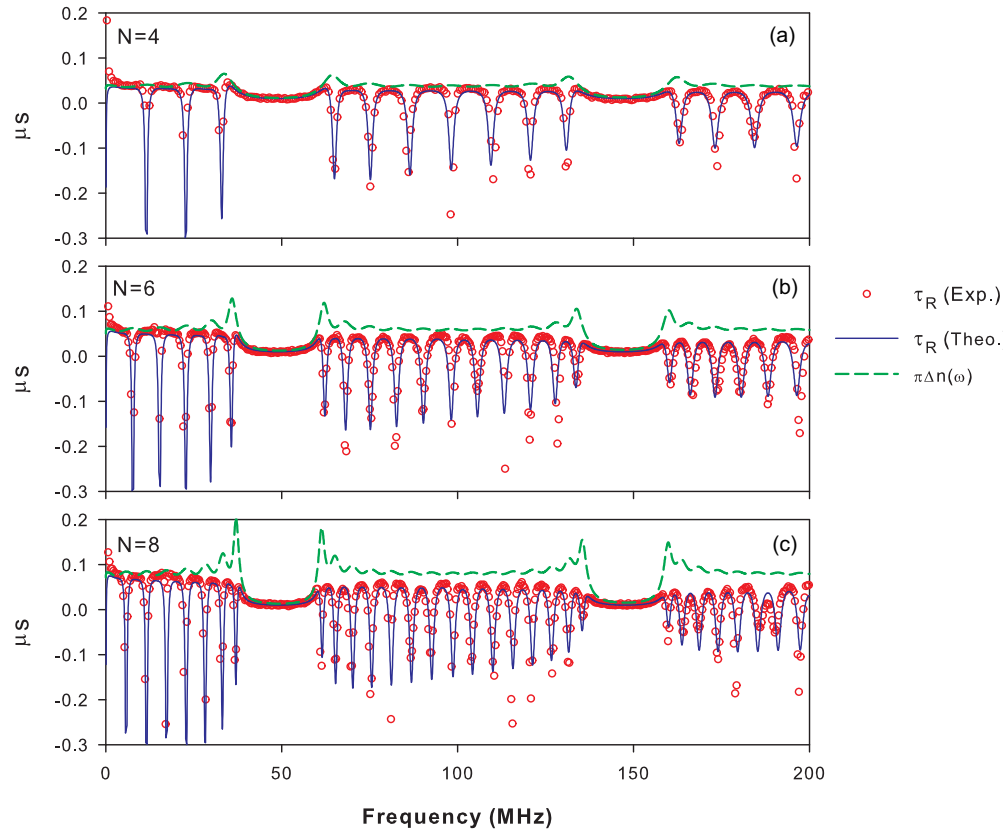

FIG. 8. Comparison between DOS (green dashed curves) and reflection delay time (blue curves) for different values of N. Red open circles give the experimental results of reflection delay time.

its both extremities as it will be detailed in the case of the vertical structure (see Sec. IV).

To summarize all the above results, we have shown analytically that for lossless media, the relationship between DOS and scattering parameters [transmission, reflection, det(S)] are exact. These results are found still valid both numerically and experimentally with a good approximation for relatively low loss systems. However, for high loss systems, the DOS represents different behaviors in comparison with the derivative of the phase of det(S_h) because of the negative peaks displayed by the latter at the band edges. Also, the relation between the absorption and |det(S_h)| [Eq. (19)] becomes no longer valid. Nevertheless, the transmission delay time (Fig. 7) still exhibits similar behaviors as the DOS and remains robust to the effect of loss.

IV. VERTICAL STRUCTURE: ANALYTICAL AND EXPERIMENTAL RESULTS

In this section, we give an analytical and experimental comparative study of DOS and scattering parameters in a finite 1D coaxial photonic crystal made of N cells attached vertically along a waveguide [Fig. 1(d)]. As in the previous section, we shall first discuss analytically the relationship between the DOS and the scattering phase for lossless media. Also, we give a comparison between the transmission and reflection delay times and DOS. The effect of loss on such relations will be discussed through an analysis of numerical and experimental results. In addition, we show that because of loss, the observed negative delta peaks associated with transmission and reflection delay times give respectively the eigenmodes of the finite system with two different boundary conditions at the bottom ($E = 0$ or $H = 0$), E and H being the electric and magnetic fields respectively.

A. Density of states and scattering phase

For the vertical system, the two semi-infinite wires are now grafted at the same site at the bottom side of the finite structure. The inverse of the Green's function of the vertical structure illustrated in Fig. 1(d) becomes

$$g_v^{-1}(M,M) = \begin{pmatrix} A_N - 2jF & B_N \\ B_N & A_N \end{pmatrix}. \tag{27}$$

The expressions of the transmission and reflection coefficients are given by [53]

$$t_v = -2jFA_N \det[g_v(M,M)] \tag{28a}$$

and

$$r_v = \left(B_N^2 - A_N^2\right)\det[g_v(M,M)], \tag{28b}$$

where

$$\det[g_v(M,M)] = \frac{1}{A_N^2 - B_N^2 - 2jFA_N}. \tag{29}$$

It is worth mentioning that the eigenmodes of the finite structure [Fig. 1(d)] are given by [53] (see Appendix A)

$$\det\left[g_v^{-1}(M,M)\right] = 0. \tag{30}$$

As mentioned above, the surface terminations (ends) of the finite crystal with electric wall ($E = 0$) on the bottom side and magnetic wall ($H = 0$) on the top side (Fig. 1(c)) are given by $A_N = 0$ [Eq. (A29)]. Therefore, from Eqs. (28a) and (29), one can deduce that these modes correspond to vanishing the vertical transmission $t_v = 0$. Similarly, the eigenmodes of the finite structure with $H = 0$ boundary condition on its both sides [Fig. 1(a)] are given by $A_N^2 - B_N^2 = 0$ [Eq. (A27)]. Therefore, from Eqs. (28b) and (29), one can deduce that these modes correspond to vanishing the vertical reflection $r_v = 0$. These results show clearly how the eigenmodes of both structures in Figs. 1(a) and 1(c) are given by $r_v = 0$ and $t_v = 0$, respectively.

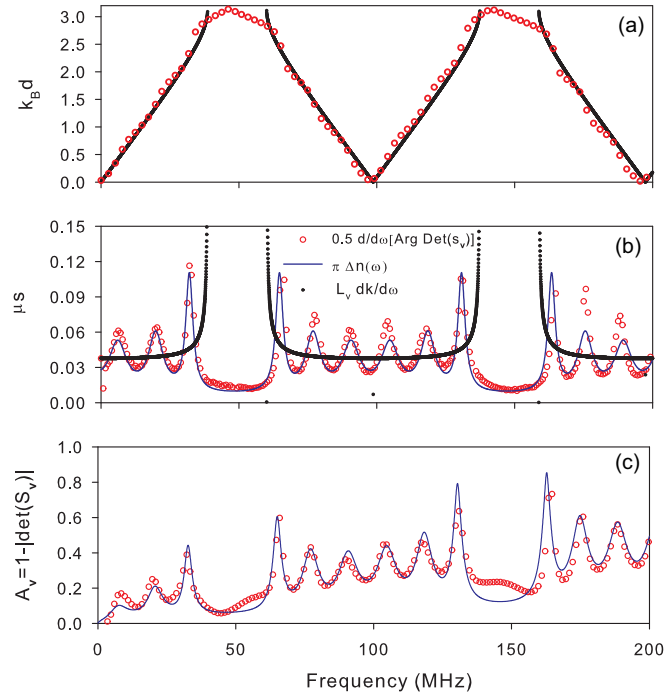

FIG. 9. Same as in Fig. 2 but for the vertical structure depicted in Fig. 1(d) with $N = 4$ cells.

All the above expressions of the transmission and reflection coefficients [Eqs. (28a) and (28b)] are different from those of the horizontal structure [Eqs. (10a) and (10b)]. However, Eqs. (15)–(19) showing how the DOS and the absorption coefficient can be extracted from the scattering parameters for the lossless horizontal structure, remain valid in the case of the vertical structure (see Appendix C), where we should only replace the subscript (h) by (v).

Figure 9 illustrates the same results as in Fig. 2 but for the vertical structure. Open circles in Fig. 9(a) give the experimental dispersion curves derived from the scattering matrix (see below). Figure 9(b) shows that the derivative of the phase of det(S_v) versus the frequency (open circles) is proportional to the variation of the DOS ($\Delta n_v(\omega)$) (solid line). In other words, the DOS can be extracted from the measurement of the phase of det(S_v). In spite of the small number of cells ($N = 4$), the DOS exhibits the same behavior that the DOS derived from the dispersion curves for the infinite periodic structure (dotted curves) depicted in Fig. 9(a) using the relation $\Delta n_v(\omega) = \frac{L_v}{\pi}\frac{dk}{d\omega}$, where L_v is the effective length of the finite vertical structure ($L_v \simeq 7.4$ m). Also, in presence of loss the absorption in the system can be extracted from det(S_v)

through the relation $A_v = 1 - |\det(S_v)|$ as it is illustrated in Fig. 9 (c). In addition, one can notice that the oscillations in DOS [Fig. 9(b)] and absorption [Fig. 9(c)] for the vertical structure, are more pronounced than those of the horizontal structure [Figs. 2(a) and 2(b)]. The experimental results (Open circles) are in very good agreement with theoretical ones (solid lines). As in section III, we have checked here also that the relation between DOS and $\frac{1}{2}\frac{d}{d\omega}\text{Arg}[\det(S_v)]$ still remains valid with a good approximation for relatively low loss systems. However, for high loss systems, the DOS and the derivative of the argument of $\det(S_v)$ present different behaviors, especially at the band edges where $\det(S_v)$ almost vanishes. Also, the absorption of the system can not be extracted from $|\det(S_v)|$.

B. Density of states and delay times

Similarly to Sec. III B, in the case of lossless media, one can deduce from Eqs. (28a) and (28b), the transmission and reflection delay times for the vertical structure as follows:

$$\tau_T^v = \frac{d\theta_T^v}{d\omega} = \frac{d}{d\omega}\text{Arg}\{\det[g_v(M,M)]\} + \pi \sum_n \left[\text{sgn}\frac{dA_N}{d\omega}|_{\omega=\omega_n}\right]\delta(\omega-\omega_n) \quad (31)$$

and

$$\tau_R^v = \frac{d\theta_R^v}{d\omega} = \frac{d}{d\omega}\text{Arg}\{\det[g_v(M,M)]\} + \pi \sum_n \left[\text{sgn}\frac{d\left(B_N^2 - A_N^2\right)}{d\omega}|_{\omega=\omega_n}\right]\delta(\omega-\omega_n). \quad (32)$$

θ_T^v and θ_R^v are the phases of the transmission and reflection coefficients, respectively. sgn means the sign function and ω_n represents the frequencies where the expressions A_N and $(B_N^2 - A_N^2)$ change sign, and the corresponding phases exhibit a jump of π.

As mentioned in Sec. IV A, the vertical structure presents transmission and reflection zeros for some frequencies given by $A_N = 0$ and $B_N^2 - A_N^2 = 0$, respectively [Eqs. (28a) and (28b)], then the corresponding phases exhibit a jump of π, and the delay times present negative delta peaks [Eqs. (31) and (32)]. Therefore, from Eqs. (15), (31), and (32), one can deduce that

$$\tau_T^v \neq \pi\,\Delta n_v(\omega) \quad (33a)$$

and

$$\tau_R^v \neq \pi\,\Delta n_v(\omega). \quad (33b)$$

The negative delta peaks of the transmission delay time induced by the second term in Eq. (31), give the eigenmodes of the system with $H = 0$ boundary condition on one side and $E = 0$ on the other side [Eq. (A29)] [Fig. 1(c)]. Whereas, the negative delta peaks associated to the reflection delay time induced by the second term in Eq. (32) give the eigenmodes of the system with $H = 0$ boundary conditions on both sides [Eq. (A27)] [Fig. 1(a)]. Equations (15), (31), and (32) show that for lossless media, apart from the existence of delta peaks in τ_R^v and τ_T^v, these latter quantities are equivalent to DOS.

However, in a lossy system, the previous Eqs. (31) and (32) still remain approximately valid. Moreover, because of loss, the true delta functions that appear in the transmission and reflection delay times broaden and become antiresonances with a Lorentzian shape easy to be detected experimentally (see below). Figure 10 presents the same results as in Fig. 5 but for the vertical structure [Fig. 1(d)]. Figure 10(b) shows that the transmission coefficient vanishes for some frequencies giving rise to abrupt phase drop [Fig. 10(c)] and therefore negative delay time [Fig. 10(d)]. The peaks of DOS [Fig. 10(e)] almost coincide with negative delta peaks in the transmission delay time which give the eigenmodes of the system described in Fig. 1(c) with $H = 0$ boundary condition on one side and $E = 0$ on the other side. These discrete modes are reported by red open circles in Fig. 10(a). One can notice that among the different modes, there exists a peak in each gap around 47 and 143 MHz; these modes are induced by the surface with electric wall (i.e., $E = 0$ boundary condition) [Fig. 1(c)]. We observe that these modes fall in the mid-gaps around $f_1 = 47$ MHz and $f_2 = 143$ MHz given by $kd_1 = \omega d_1\sqrt{\varepsilon}/c = (2n+1)\pi/2$ (n is an integer). These surface modes do not appear in the DOS [Fig. 10(e)]. In order to show the spatial localization of these modes, we have presented in Fig. 11 the square modulus of the electric field as function of the space positions $x(m)$ along the finite structure depicted in Fig. 1(c) for the two surface modes at $f_1 = 47.68$ MHz and $f_2 = 143.67$ MHz [labeled 1 and 2 respectively in Fig. 10(a)]. As predicted, these two modes are localized at the surface of the structure and decrease in the bulk. In particular, the electric field vanishes at the surface because of $E = 0$ boundary condition at this point. Also, the number of oscillations in each cell increases for high frequencies [Fig. 11(b)]. The penetration depth δ of the electric field in Fig. 11 can be deduced from the decay of the amplitude of oscillations between two periods, and gives $\delta = 2.9$ m. This quantity is almost the same as the one obtained from the value of the imaginary part of the wave number in the center of the gap in Fig. 10(a), namely, $\delta' = 2.92$ m. The fast decay of the electric field (almost one period) is due to the frequency position of the surface mode in the middle of the gap. Similarly to Fig. 5, the behavior of the transmission delay time versus the frequency in absence of dissipation is plotted in Fig. 10(f). We can see clearly that, apart the true delta peaks indicated by vertical bars, the transmission delay time is equivalent to the DOS [Fig. 10(e)].

The reflection spectra exhibit the same behavior as the transmission spectra as it is illustrated in Figs. 10(b) and 10(h). Similarly to the transmission coefficient, the negative delta peaks associated to the reflection coefficient [Fig. 10(j)] give the eigenmodes of the finite structure when the boundary conditions are $H = 0$ on both sides [Fig. 1(a)]. These modes are reported by red open circles in Fig. 10(g). Also, one can notice the absence of surface modes in the gaps [Figs. 10(g) and 10(j)]. Indeed, the surface termination with $H = 0$ boundary conditions do not support surface modes [54]. Also, it is worth noticing that the surface modes of the finite structure are almost the same as the surface modes of the semi-infinite structure. The latter are given by [54] $kd_1 = \pi/2, 3\pi/2, \ldots$ (i.e., $f = 49$ and 147 MHz). For both structures, one can notice that the DOS is different from τ_T [Figs. 10(d) and 10(e)] and τ_R [Figs. 10(j) and 10(k)] because of the existence of negative delta peaks induced by the terms A_N and $A_N^2 - B_N^2$

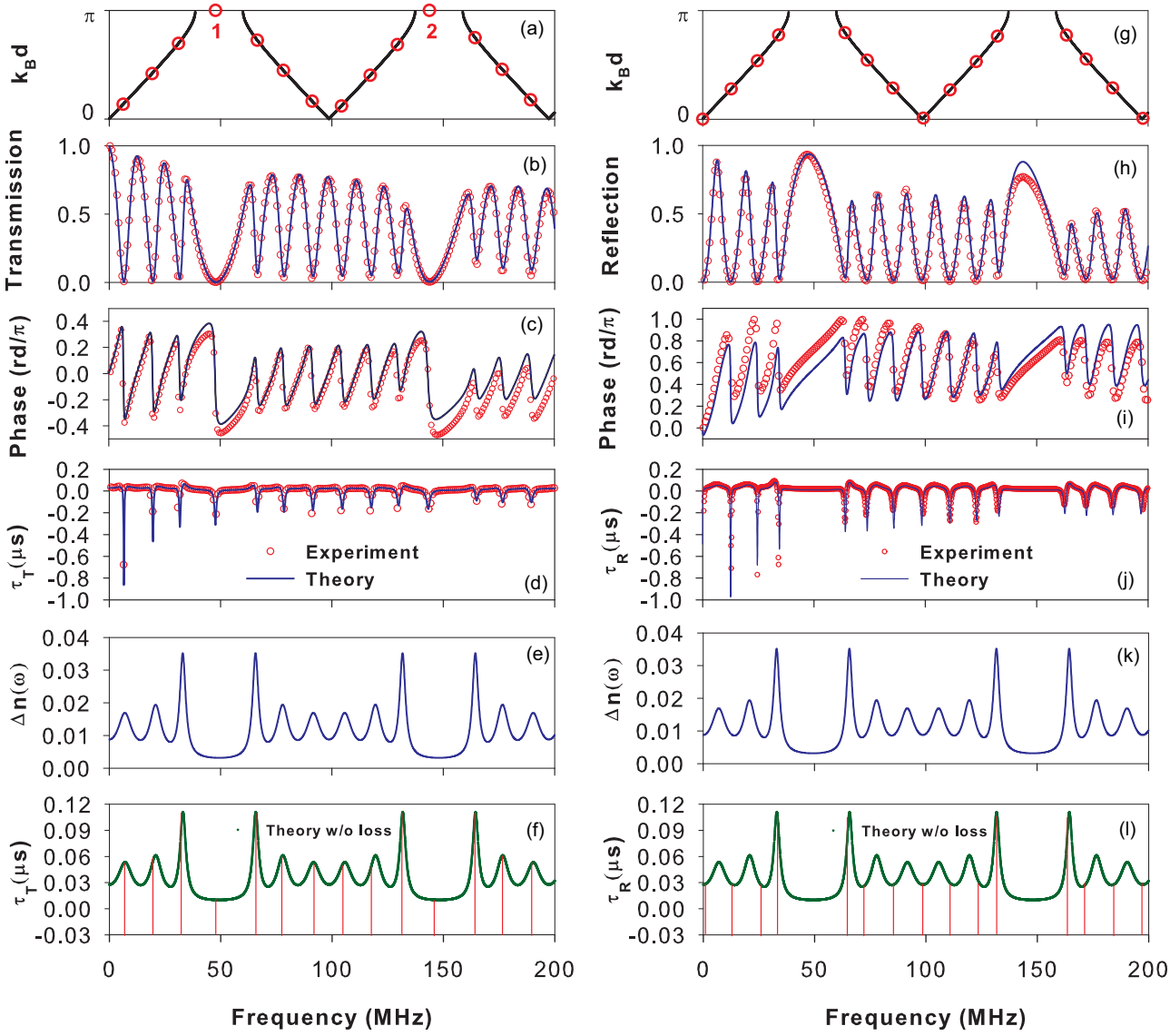

FIG. 10. Same as in Figs. 5 and 6 but for transmission (left panel) and reflection (right panel) coefficients of the vertical structure depicted in Fig. 1(d) with N = 4 cells. It is worth noticing that (d) and (f) (left) and (j) and (l) (right) are not plotted with the same scale.

[Eqs. (31) and (32)], respectively. Let us mention here also that the above analytical demonstrations suppose that A_N and B_N [Eqs. (3a) and (3b)] are real quantities which is the case for lossless media. However, we have checked numerically (see Fig. 15 in Appendix I) that even in presence of loss the real part of A_N and $A_N^2 - B_N^2$ still vanish at the frequencies of the eigenmodes of the finite system, which do not affect the frequency positions of the peaks in the delay times, whereas the imaginary part of A_N and $A_N^2 - B_N^2$ slightly increases when increasing loss. This quantity is responsible of the broadening of the delta peaks in the delay time. These results clearly show that even in presence of loss, the frequency positions of the eigenmodes of the finite system are almost unaffected, while the broadening of these resonances in the delay time enables to detect easily these modes. This is the case for the modes in Figs. 10(d) and 10(j). The behavior of the reflection delay time versus the frequency in absence of dissipation is plotted in Fig. 10(l). We can see clearly that, apart the true delta peaks indicated by vertical bars, the reflection delay time is equivalent to the transmission delay time [Fig. 10(f)] and to the DOS [Fig. 10(k)].

V. CONCLUSION

In this paper, we have presented a comparative study of DOS and scattering parameters (argument and modulus of the scattering matrix S) for a finite 1D coaxial photonic crystal made of N cells attached either horizontally or vertically along a waveguide (Fig. 1). For both structures, we have demonstrated analytically that for lossless systems, the DOS is proportional to the derivative of the argument of $\det(S)$, the so-called Friedel phase [17]. This proportionality remain valid with a good approximation for relatively low loss systems, which enables us to extract experimentally the DOS and therefore the dispersion curves. Also, the absorption coefficient can be extracted from the modulus of $\det(S)$. However, for high

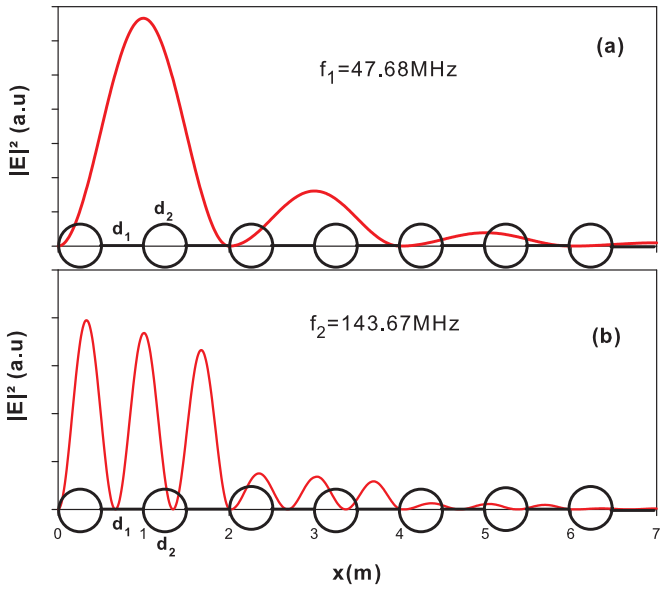

FIG. 11. Square modulus of the electric field (in arbitrary units) as function of the space positions $x(m)$ along the finite structure depicted in Fig. 1(c) for the two surface modes at $f_1 = 47.68$ MHz (a) and $f_2 = 143.67$ MHz (b) labeled 1 and 2 in Fig. 10(a).

loss systems, these relations are no longer valid. Nevertheless, we have shown that the transmission delay time for the horizontal structure describes very well the DOS even for high loss systems. In addition, we have shown that the reflection delay time is different from the DOS because of the negative delta peaks due to reflection zeros. These results complete our previous theoretical predictions, where we have shown that the reflection and transmission delay times for a lossless symmetric superlattice are equivalent, and are directly proportional the DOS [45]. Indeed, we have shown analytically that, apart from the negative delta peaks that may exist in the delay times, the transmission and reflection delay times are equivalent and proportional to the DOS. In presence of loss, the delta peaks in the delay times become broadened which enables their easy observation in experiments. Therefore, the reflection delay time shows different behaviors versus the frequency for the horizontal structure can become different from the DOS. In addition, for the vertical structure, we have demonstrated that the negative delta peaks associated to the transmission coefficient give the eigenmodes of the system with $H = 0$ boundary condition on one side and $E = 0$ on the other side. However, the negative delta peaks associated to the reflection coefficient give the eigenmodes of the finite structure with $H = 0$ boundary condition on both sides. H and E being the magnetic and electric fields, respectively. The analytical results are obtained within the framework of the Green's function method [5,53], and the experiments are carried out using coaxial cables in the radio-frequency regime. All the above results show that both (horizontal and vertical) structures give almost similar results about the DOS of the system for lossless media, however the vertical structure exhibits additional informations as it enables to extract also the confined and surface modes of the photonic crystal with different boundary conditions on its extremities. The results presented here for the photonic crystal are valid for any photonic structure characterized by two network ports, all we need consists in changing the elements of the Green's function in Eq. (2) by the appropriate values of a given photonic system. Also, these results can be transposed straightforwardly to acoustic waves in slender tubes [65], mesoscopic quantum waveguides [66], and spin waves in magnonic circuits [67] as the mathematical equations governing all these excitations are isomorphic.

ACKNOWLEDGMENTS

The authors would like to thank the anonymous referees for their constructive comments which enable the improvement of the quality of this paper.

APPENDIX A: GREEN'S FUNCTION APPROACH

The calculation method used in this work is the interface response theory of continuous media [5,53], which allows us to calculate the Green's function of any composite material. The knowledge of the Green's function enables us to deduce the different properties of the system such as the dispersion relation, transmission and reflection coefficients as well as density of states (DOS). The Green's function of any composite system can be deduced from the juxtaposition of the Green's function of the elementary constituents of the system. In what follows, we give the basic concept and the fundamental equations of this method.

Let us consider any composite material contained in its space of definition D and formed out of N different homogeneous pieces located in their domains D_i. Each piece is bounded by an interface M_i, adjacent in general to j ($1 \leqslant j \leqslant J$) other pieces through subinterface domains M_{ij}. The ensemble of all these interface spaces M_i will be called the interface space M of the composite material. The elements of the Green's function $g(DD)$ of any composite material can be obtained from [68]

$$g(DD) = G(DD) - G(DM)G^{-1}(MM)G(MD) + G(DM)G^{-1}(MM)g(MM)G^{-1}(MM)G(MD), \tag{A1}$$

where $G(DD)$ is the reference Green's function formed out of truncated pieces in D_i of the bulk Green's functions of the infinite continuous media and $g(MM)$, the interface element of the Green's function of the composite system.

The knowledge of the inverse of $g(MM)$ is sufficient to calculate the interface states of a composite system through the relation [68]

$$\det[g^{-1}(MM)] = 0. \tag{A2}$$

Moreover if $U(D)$ represents an eigenvector of the reference system, Eq. (A1) enables the calculation of the eigenvectors $u(D)$ of the composite material as

$$u(D) = U(D) + G(DM) \times [G^{-1}(MM)g(MM)G^{-1}(MM) - G^{-1}(MM)]U(M), \tag{A3}$$

In Eq. (A3), $U(D)$, $U(M)$, and $u(D)$ are row vectors. Equation (A3) provides a description of all the waves reflected and transmitted by the interfaces, as well as the reflection

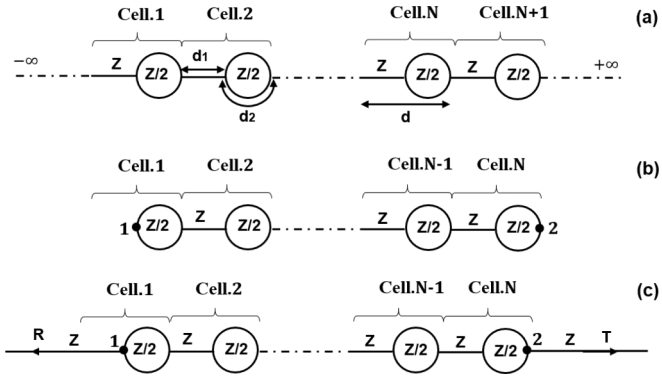

FIG. 12. (a) The infinite periodic structure made of a wire of length d_1 and a loop formed out by two wires, each of length d_2, $d = d_1 + d_2$ is the period of the structure. (b) The finite periodic structure containing N cells with loop termination on both sides. (c) The finite periodic structure inserted between two semi-infinite wires.

and transmission coefficients of the composite system. In this case, $U(D)$ is a bulk wave launched in one homogeneous piece of the composite material [69].

The periodic structure is made of N cells, each cell is composed of a wire of length d_1 and a loop formed out by two wires, each of length d_2, $d = d_1 + d_2$ is the period of the photonic crystal. In what follows, we give the detailed analytical calculation of the Green's functions of the infinite, semi-infinite and finite wires which represent the elementary constituents of any photonic crystal under study (Fig. 12).

We consider an infinite homogeneous isotropic dielectric wire characterized by its characteristic impedance Z. In the limit where the widths of the wires are much smaller than their lengths, the telegrapher's equation describing microwave networks, the so-called TEM waves, is given by

$$\left[\frac{\partial^2}{\partial x^2} + k^2\right] E(x) = 0, \tag{A4}$$

where

$$k = \frac{\omega}{c}\sqrt{\varepsilon(\omega)}. \tag{A5}$$

k is the wave number, which is directed along the direction of the wire, ω the angular frequency of the wave, c the speed of light in vacuum, $\varepsilon(\omega)$ the relative permittivity, and $j = \sqrt{-1}$. The Green's function between any two points x and x' of the infinite wire is defined by

$$F\left[\frac{\partial^2}{\partial x^2} + k^2\right] G(x, x') = \delta(x - x'), \tag{A6}$$

where

$$F = \frac{\omega}{Z}. \tag{A7}$$

The solution of Eq. (A6) is given by [70]

$$G(x, x') = -j\frac{e^{-jk|x-x'|}}{2F}, \tag{A8}$$

The inverse of the Green's function in the interface space $M = \{\frac{-d_1}{2}, \frac{+d_1}{2}\}$ of a wire of length d_1 is given by a (2×2) matrix under the following form [70]:

$$g_1^{-1}(M, M) = \begin{pmatrix} a & b \\ b & a \end{pmatrix}, \tag{A9}$$

where $a = -jF\frac{C_1}{S_1}$, $b = jF\frac{1}{S_1}$, $C_1 = \cos(kd_1)$, and $S_1 = j\sin(kd_1)$.

Similarly, the inverse of the Green's function of a symmetric loop formed out by two finite wires of length d_2 in the interface space $M = \{\frac{-d_2}{2}, \frac{+d_2}{2}\}$ is given by

$$g_2^{-1}(M, M) = \begin{pmatrix} A & B \\ B & A \end{pmatrix}, \tag{A10}$$

where $A = -j2F\frac{C_2}{S_2}$, $B = j2F\frac{1}{S_2}$, $C_2 = \cos(kd_2)$, and $S_2 = j\sin(kd_2)$. One can see that the symmetric loop is equivalent to a wire of length d_2 and impedance $Z/2$.

Also, we shall need the inverse Green's function of the semi-infinite wires characterized by the impedance Z at the extremities of the finite system [Fig. 12(c)], namely,

$$g_s^{-1}(1, 1) = g_s^{-1}(2, 2) = -jF \tag{A11}$$

where $F = \frac{\omega}{Z}$.

1. Green's function and dispersion relation of an infinite photonic crystal

The Green's function of the infinite structure [Fig. 12(a)] is obtained by a linear superposition of the (2×2) matrices [Eqs. (A9) and (A10)] at different interfaces leading to an infinite tridiagonal matrix,

$$g^{-1}(M, M) = \begin{pmatrix} \ddots & \ddots & \ddots & & & & & & & & \\ & b & A+a & B & & & & & & & \\ & & B & A+a & b & & & & & & \\ & & & b & A+a & B & & & & & \\ & & & & \ddots & \ddots & \ddots & & & & \\ & & & & & \ddots & A+a & B & & & \\ & & & & & & B & A+a & b & & \\ & & & & & & & b & A+a & B & \\ & & & & & & & & B & A+a & b \\ & & & & & & & & & \ddots & \ddots & \ddots \end{pmatrix}. \tag{A12}$$

After a Fourier transform of the above tridiagonal matrix within one unit cell defined in the space $M_c = \{(n, i = 1, \frac{-d_1}{2}), (n, i = 1, \frac{+d_1}{2})\}$, one obtains [71]

$$g_c^{-1}(k_B, M_c M_c) = \begin{pmatrix} a + A & b + B\exp(-jk_B d) \\ b + B\exp(jk_B d) & a + A \end{pmatrix}. \tag{A13}$$

Here, k_B is the Bloch wave number of the infinite periodic structure (note that k_B is real inside the pass bands and complex inside the gaps of the infinite system). From the previous matrix, one can deduce the dispersion relation of the infinite photonic crystal [Fig. 12(a)] from the equation $\det(g_c^{-1}(k_B, MM)) = 0$ [Eq. (A13)], namely,

$$\cos(k_B d) = \cos(kd_1)\cos(kd_2) - \tfrac{5}{4}\sin(kd_1)\sin(kd_2). \tag{A14}$$

It is also straightforward to Fourier analyze back into real space all the elements of $g_c(k_B, MM)$ and obtain the interface elements of g in the following form [71]:

$$g(n, 1, +d_1/2; n', 1, +d_1/2) = g(n, 1, -d_1/2; n', 1, -d_1/2) = -\frac{(A + a)}{Bb}\frac{t^{|n-n'|+1}}{t^2 - 1}, \tag{A15a}$$

$$g(n, 1, -d_1/2; n', 1, +d_1/2) = \frac{t^{|n-n'|+1}}{B(t^2 - 1)} + \frac{t^{|n-n'-1|+1}}{b(t^2 - 1)}, \tag{A15b}$$

$$g(n, 1, +d_1/2; n', 1, -d_1/2) = \frac{t^{|n-n'|+1}}{B(t^2 - 1)} + \frac{t^{|n-n'+1|+1}}{b(t^2 - 1)}, \tag{A15c}$$

where the integers n and n' refer to the cell number $-\infty \leqslant n, n' \leqslant +\infty$, and the parameter t represents $e^{jk_B d}$ and is defined by

$$t = \eta + \sqrt{\eta^2 - 1} \text{ if } \eta < -1, \tag{A16a}$$

$$t = \eta + j\sqrt{1 - \eta^2} \text{ if } |\eta| \leqslant 1, \tag{A16b}$$

$$t = \eta - \sqrt{\eta^2 - 1} \text{ if } \eta > 1, \tag{A16c}$$

where $\eta = \cos(k_B d)$.

2. Green's function and eigenmodes of a finite photonic crystal

The finite structure containing N equidistant loops [Fig. 12(b)] is cut out from the infinite periodic structure [Fig. 12(a)] and this piece is subsequently connected at its extremities $M_0 = \{(n = 1, i = 1, \frac{+d_1}{2}), (n = N + 1, i = 1, \frac{-d_1}{2})\}$ to two semi-infinite wires [Fig. 12(c)]. The finite system in Fig. 12(b) can be subtracted from the infinite system by eliminating the segments lying in the space of interface $M_s = \{(n = 1, i = 1, \frac{-d_1}{2}), (n = 1, i = 1, \frac{+d_1}{2}), (n = N + 1, i = 1, \frac{-d_1}{2}), (n = N + 1, i = 1, \frac{+d_1}{2})\}$. Therefore, one obtains an infinite tridiagonal matrix $g_d^{-1}(M, M)$ defined in the interface domain of all the sites n $(-\infty \leqslant n \leqslant +\infty)$ and composed of three decoupled submatrices associated with two semi-infinite systems and a finite system as follows:

$$g_d^{-1}(M, M) = \begin{pmatrix} \ddots & \ddots & \ddots & & & & & & & & \\ & b & A + a & B & & & & & & & \\ & & B & A & 0 & & & & & & \\ & & & 0 & A & B & & & & & \\ & & & & \ddots & \ddots & \ddots & & & & \\ & & & & & \ddots & A + a & B & & & \\ & & & & & & B & A & 0 & & \\ & & & & & & & 0 & A & B & \\ & & & & & & & & B & A + a & b \\ & & & & & & & & & \ddots & \ddots & \ddots \end{pmatrix}. \tag{A17}$$

This matrix is similar to the one associated to the infinite photonic crystal. Only the elements associated to the interface space M_s are different. The cleavage operator [5], which enables to cut the finite system [Fig. 12(b)] from the infinite one [Fig. 12(a)], is therefore, a (4×4) matrix in the interface space M_s and can be obtained from the following expression:

$$V(M_s, M_s) = g_d^{-1}(M, M) - g^{-1}(M, M) = \begin{pmatrix} -a & -b & 0 & 0 \\ -b & -a & 0 & 0 \\ 0 & 0 & -a & -b \\ 0 & 0 & -b & -a \end{pmatrix}, \tag{A18}$$

where a and b are given by Eq. (A9). The Green's function in the interface space M_s of the infinite periodic structure can be obtained from Eq. (A15) as follows:

$$g(M_s, M_s) = \frac{t}{t^2-1}\begin{pmatrix} -\frac{A+a}{Bb} & \frac{b+Bt}{Bb} & -\frac{A+a}{Bb}t^N & \frac{b+Bt}{Bb}t^N \\ \frac{b+Bt}{Bb} & -\frac{A+a}{Bb} & \frac{b+Bt}{Bb}t^{N-1} & -\frac{A+a}{Bb}t^N \\ -\frac{A+a}{Bb}t^N & \frac{b+Bt}{Bb}t^{N-1} & -\frac{A+a}{Bb} & \frac{b+Bt}{Bb} \\ \frac{b+Bt}{Bb}t^N & -\frac{A+a}{Bb}t^N & \frac{b+Bt}{Bb} & -\frac{A+a}{Bb} \end{pmatrix}. \tag{A19}$$

The knowledge of the cleavage operator [Eq. (A18)] and the Green's function $g(M_s, M_s)$ [Eq. (A19)] allows us to deduce the operator $\Delta(M_s, M_s)$ as follows:

$$\Delta(M_s, M_s) = I(M_s, M_s) + V(M_s, M_s)g(M_s, M_s). \tag{A20}$$

In order to calculate the Green's function on both ends of the finite structure illustrated in Fig. 12(b), we only need the truncated matrix $\Delta(M_0, M_0)$ in the interface space $M_0 = \{(n=1, i=1, \frac{+d_1}{2}), (n=N+1, i=1, \frac{-d_1}{2})\}$,

$$\Delta(M_0, M_0) = \begin{pmatrix} 1-\frac{t}{t^2-1}\frac{Y_1}{Bb} & -\frac{t^N}{t^2-1}\frac{Y_2}{Bb} \\ -\frac{t^N}{t^2-1}\frac{Y_2}{Bb} & 1-\frac{t}{t^2-1}\frac{Y_1}{Bb} \end{pmatrix}, \tag{A21}$$

where

$$Y_1 = b^2 - a^2 - aA + Bbt \text{ and } Y_2 = aB - Abt. \tag{A22}$$

The inverse Green's function $g_0^{-1}(M_0, M_0)$ in the interface space M_0 of the finite periodic structure illustrated in Fig. 12(b) is given by

$$g_0^{-1}(M_0, M_0) = \Delta(M_0, M_0)g^{-1}(M_0, M_0), \tag{A23}$$

where $g^{-1}(M_0, M_0)$ is obtained by inverting the truncated Green's function in the interface space M_0, namely,

$$g(M_0, M_0) = \frac{t}{t^2-1}\begin{pmatrix} -\frac{A+a}{Bb} & \frac{b+Bt}{Bb}t^{N-1} \\ \frac{b+Bt}{Bb}t^{N-1} & -\frac{A+a}{Bb} \end{pmatrix}. \tag{A24}$$

From Eqs. (A21), (A23), and (A24), we obtain

$$g_0^{-1}(M_0, M_0) = \begin{pmatrix} A_N & B_N \\ B_N & A_N \end{pmatrix}, \tag{A25}$$

where

$$A_N = \frac{Y_1}{(A+a)\Delta}\left[\Delta - Bb\left(t - \frac{1}{t}\right)Y_1\right], \tag{A26a}$$

$$B_N = Bb\left(t - \frac{1}{t}\right)\frac{Y_1Y_2}{(A+a)\Delta}t^{(N-1)}, \tag{A26b}$$

and

$$\Delta = Y_1^2 - Y_2^2 t^{2(N-1)}. \tag{A26c}$$

The eigenmodes of the photonic crystal with $H = 0$ boundary conditions on both sides [Fig. 1(a)] are given by

$$\det\left[g_0^{-1}(M, M)\right] = A_N^2 - B_N^2 = 0. \tag{A27}$$

Similarly, we can show that the eigenmodes of the finite photonic crystal with $E = 0$ boundary conditions on both sides are given by

$$\Delta = [Y_1 - Y_2 t^{(N-1)}][Y_1 + Y_2 t^{(N-1)}] = 0. \tag{A28}$$

Finally, the eigenmodes of the finite structure with $E = 0$ boundary condition on its bottom side and $H = 0$ on its top side [Fig. 1(c)] are given by

$$A_N = 0. \tag{A29}$$

APPENDIX B: EXPERIMENTAL SETUP

The experimental setup used in this study consists of standard coaxial cables RG-58/U of different lengths with the same characteristic impedances $Z = 50\ \Omega$. The segments of coaxial cables were connected by standard BNC T connectors. The cables were filled with polyethylene ($\varepsilon' = 2.3$), corresponding to a nominal propagation speed of $0.66c$. The boundary conditions at the surfaces of the finite 1D photonic crystal [Figs. 1(a) and 1(c)] can be either $E = 0$ (i.e., electric wall) or $H = 0$ (i.e., magnetic wall). The attenuation in the coaxial cables was simulated by introducing a complex dielectric permittivity $\varepsilon = \varepsilon' + j\varepsilon''$. The attenuation coefficient α'' can be expressed as $\alpha'' = \varepsilon''\omega/c\sqrt{\varepsilon'}$. On the other hand, the attenuation specification data supplied by the manufacturer of the coaxial cables based on energy decreasing of the waves along the cables in the frequency range of 10–200 MHz, can be approximately fitted with the expression $\ln(\alpha'') = \gamma + \beta\ln(\omega)$, where γ and β are two constants. From this fitting procedure, a useful expression for ε'' as a function of frequency can be obtained under the form $\varepsilon'' = (\frac{f}{f_0})^{-0.5}$, where the frequency f is expressed in Hz and $f_0 = 9200$ Hz. The scattering matrix S of the 1D photonic crystal was measured in the frequency range 1–200 MHz by means of a broadband vector network analyzer (VNA) Agilent PNA-X N5242A. The VNA allows accurate forward and reverse measurements on the device under test, which are needed to characterize all the four S parameters. The resolution of amplitude and phase measurement is around 0.5 mV and 0.01°, respectively using an intermediate frequency filter bandwidth of 1 KHz (IF). The dynamic range is around 100 dB. The noise of the VNA at GHz frequency is two small (0.01 mV rms) and is drastically reduced by the IF filter. The measured S parameters are accurate and reliable and the error is less than 0.2%.

APPENDIX C: TRANSMISSION AND REFLECTION COEFFICIENTS FOR LOSSLESS SYSTEMS

The Green's function method allows us to calculate the reflection and transmission coefficients through the finite size photonic crystal. The inverse of the Green's function of the final structure in the interface space $M = \{1, 2\}$ [Fig. 12(c)] can be obtained from Eqs. (A11) and (A25), namely,

$$g_h^{-1}(M, M) = \begin{pmatrix} A_N - jF & B_N \\ B_N & A_N - jF \end{pmatrix}. \tag{C1}$$

The Green's function enables us to determine the transmission and reflection coefficients through the finite structure. These latter quantities are obtained by inverting the above matrix in Eq. (C1), namely,

$$g_h(M,M) = \det[g_h(M,M)]\begin{pmatrix} A_N - jF & -B_N \\ -B_N & A_N - jF \end{pmatrix}, \quad \text{(C2)}$$

where

$$\det[g_h(M,M)] = \frac{1}{A_N^2 - B_N^2 - F^2 - 2jFA_N}. \quad \text{(C3)}$$

Let us consider an incident wave $U(x) = e^{-jkx}$ launched from the left side of the finite structure [Fig. 1(b)]. With the help of Eq. (A3), one can find the transmitted wave

$$u_T(x) = G(x,1)G^{-1}(1,1)g_h(1,2)G^{-1}(2,2) = t_h e^{-jkx}, \quad \text{(C4)}$$

where t_h is the transmission coefficient. Labels 1 and 2 in the Green's functions mean the space of interfaces related to the entrance and the exit of the system. From Eqs. (A8), (C2), and (C4) one can deduce,

$$t_h = -2jF g_h(1,2), \quad \text{(C5)}$$

where

$$g_h(1,2) = -B_N \det[g_h(M,M)]. \quad \text{(C6)}$$

By the same way, the reflected wave is given by

$$u_R(x) = G(x,1)\{G^{-1}(1,1)g_h(1,1)G^{-1}(1,1) - G^{-1}(1,1)\} = r_h e^{jkx}, \quad \text{(C7)}$$

where r_h is the reflection coefficient. From Eqs. (A8), (C2), and (C7) one can deduce

$$r_h = -1 - 2jF g_h(1,1). \quad \text{(C8)}$$

By replacing $g_h(1,1) = (A_N - jF)\det[g_h(M,M)]$ by its expression using Eq. (C3) and from Eq. (C8), one obtains the reflection coefficient in an explicit form

$$r_h = -C_N \det[g_h(M,M)], \quad \text{(C9)}$$

where C_N is given by

$$C_N = A_N^2 - B_N^2 + F^2 = j2\left(A_1^2 - B_1^2 + F^2\right)\left(Y_1^2 - Y_2^2\right)t^{N-2}\sin(Nk_B d). \quad \text{(C10)}$$

Equations (C5) and (C8) are equivalent to the well-known Fisher-Lee relation [2,72] relating the Green's function and the scattering matrix elements.

It is worth mentioning that in lossless sytem, A_N and B_N [Eqs. (A26a) and (A26b)] are real quantities. Therefore, from the expressions of t_h [Eq. (10a)] and r_h [Eq. (10b)] (Sec. III A), one can deduce easily the transmission and reflection rates, respectively,

$$T_h = |t_h|^2 = \frac{(2FB_N)^2}{\left(A_N^2 - B_N^2 - F^2\right)^2 + (2FA_N)^2} = \frac{(2FB_N)^2}{\left(A_N^2 - B_N^2 + F^2\right)^2 + (2FB_N)^2}, \quad \text{(C11)}$$

$$R_h = |r_h|^2 = \frac{C_N^2}{\left(A_N^2 - B_N^2 - F^2\right)^2 + (2FA_N)^2} = \frac{\left(A_N^2 - B_N^2 + F^2\right)^2}{\left(A_N^2 - B_N^2 + F^2\right)^2 + (2FB_N)^2}. \quad \text{(C12)}$$

From Eqs. (C11) and (C12), we can show that in absence of loss, T_h and R_h verify the conservation energy $T_h + R_h = 1$.

By the same way, from Eqs. (28a) and (28b) (Sec. IV A), one can determine the transmission and reflection rates for the vertical system, respectively,

$$T_v = |t_v|^2 = \frac{(2FA_N)^2}{\left(A_N^2 - B_N^2\right)^2 + (2FA_N)^2}, \quad \text{(C13)}$$

$$R_v = |r_v|^2 = \frac{\left(A_N^2 - B_N^2\right)^2}{\left(A_N^2 - B_N^2\right)^2 + (2FA_N)^2}. \quad \text{(C14)}$$

From Eqs. (C13) and (C14), it is clear that T_v and R_v verify the conservation energy $T_v + R_v = 1$.

APPENDIX D: Arg[det(S_h)] AND Arg[det(S_v)] FOR LOSSLESS SYSTEMS

For lossless systems, the determinant of the scattering matrix S_h [Eq. (16)] for the horizontal system (Sec. III A) can be derived from the expressions of t_h and r_h [Eqs. (10a) and (10b)] as follows:

$$\det(S_h) = r_h^2 - t_h^2 = \left\{C_N^2 + (2FB_N)^2\right\}\{\det[g_h(M,M)]\}^2, \quad \text{(D1)}$$

where the expression of $\det[g_h(M,M)]$ is given by Eq. (C3). From Eq. (D1) and after some algebraic calculation, one can find that

$$\det(S_h) = [(A_N - B_N)^2 + (F)^2][(A_N + B_N)^2 + (F)^2]\{\det[g_h(M,M)]\}^2. \quad \text{(D2)}$$

Equation (D2) clearly shows that the argument of the first term in Eq. (D2) vanishes, and therefore,

$$\text{Arg}[\det(S_h)] = 2\text{Arg}\{\det[g_h(M,M)]\}. \quad \text{(D3)}$$

By the same way, for the vertical system (Sec. IV), the determinant of the scattering matrix S_v can be deduced from the expressions of t_v and r_v [Eqs. (28a) and (28b)] such as

$$\det(S_v) = r_v^2 - t_v^2 = \left\{\left(B_N^2 - A_N^2\right)^2 + (2FA_N)^2\right\}\{\det[g_v(M,M)]\}^2, \quad \text{(D4)}$$

where the expression of $\det[g_v(M,M)]$ is given by Eq. (29) in Sec. IV A.

From Eq. (D4) and after some algebraic calculation, one can find that

$$\det(S_v) = \left\{A_N^2 - B_N^2 + 2jF\right\}\{\det[g_v(M,M)]\}. \quad \text{(D5)}$$

The first term in Eq. (D5) is the complex conjugate of $\det[g_v^{-1}(M,M)]$, and therefore,

$$\text{Arg}[\det(S_v)] = 2\text{Arg}\{\det[g_v(M,M)]\}. \quad \text{(D6)}$$

APPENDIX E: $|\det(S_h)| = T_h + R_h = 1$ FOR LOSSLESS SYSTEMS

In what follows we shall check the well known property of $\det(S)$, namely $|\det(S_h)| = T_h + R_h = 1$. From Eq. (D1), we can deduce for lossless systems the modulus of $\det(S_h)$ as follows:

$$|\det(S_h)| = \frac{C_N^2 + (2FB_N)^2}{\sqrt{\left[\left(A_N^2 - B_N^2 - F^2\right)^2 - (2FA_N)^2\right]^2 + \left[4FA_N\left(A_N^2 - B_N^2 - F^2\right)\right]^2}}. \tag{E1}$$

By developing Eq. (E1), we find

$$|\det(S_h)| = \frac{C_N^2 + (2FB_N)^2}{\left(A_N^2 - B_N^2 - F^2\right)^2 + (2FA_N)^2}. \tag{E2}$$

From Eqs. (C11), (C12), and (D1), we can deduce that $|\det(S_h)| = T_h + R_h = 1$. Similarly, from Eqs. (28a), (28b), and (D4), one can demonstrate that $|\det(S_v)| = T_v + R_v = 1$.

It should be pointed out that for low loss media, the absorption can be extracted from the modulus of the determinant of the scattering matrix through the relation $A_{h,v} \simeq 1 - |\det(S_{h,v})|$, where the subscripts h and v refer to the horizontal or vertical structure respectively.

APPENDIX F: THE TOTAL DENSITY OF STATES DOS

The total DOS of the system is obtained by integrating over x and summing on n and i the local density $n(\omega^2; n, i, x)$. For the horizontal system [Fig. 12(b)], the finite structure is placed between two semi-infinite wires. The expression of DOS can be written as the sum of three contributions [60],

$$\Delta n_T(\omega^2) = n_1(\omega^2) + 2n_2(\omega^2) + 2\Delta n_s(\omega^2), \tag{F1}$$

where $n_1(\omega^2)$ and $n_2(\omega^2)$ are the contributions of wires 1 and 2 of the photonic crystal, respectively, and $\Delta n_s(\omega^2)$ comes from the two semi-infinite waveguides surrounding the photonic crystal. The explicit expressions of the three quantities in Eq. (F1) are given by [60]

$$n_1(\omega^2) = \frac{-\varepsilon}{\pi}\mathrm{Im}\frac{t}{F(t^2-1)}\left(\frac{t(1-t^{2(N-1)})}{(t^2-1)}\frac{Y}{\Delta^-}\left\{\frac{-3}{2}d_1S_2 + \frac{4S_1}{F}Y_1^a\right\} + \frac{(N-1)\Delta^+}{\Delta^-}\left\{\frac{-3S_1S_2}{F} + 2d_1Y_1^a\right\}\right), \tag{F2}$$

$$n_2(\omega^2) = \frac{-\varepsilon}{\pi}\mathrm{Im}\frac{t}{F(t^2-1)}\left(\frac{(1-t^{2N})}{(t^2-1)}\frac{Y}{\Delta^-}\left\{\frac{3}{4}d_2S_1 + \frac{S_2}{F}Y_2^a\right\} + \frac{N\Delta^+}{\Delta^-}\left\{\frac{3}{4}\frac{S_1S_2}{F} + d_2Y_2^a\right\}\right), \tag{F3}$$

and

$$\Delta n_s(\omega^2) = \frac{-\varepsilon}{\pi}\mathrm{Im}\frac{1}{2F}\left\{\frac{1}{2F} + \frac{1}{F}\left[\frac{1}{\Delta^-}\left(\frac{t^2-1}{t} + Y_1^b\right)(2C_2S_1 + C_1S_2) - t^{2(N-1)}Y_2^b(2S_1 + S_2t)\right]\right\}, \tag{F4}$$

where

$$Y = \left(\frac{t^2-1}{t} + Y_1^s\right)Y_2^b + \left(\frac{t^2-1}{t} + Y_1^b\right)Y_2^s, \tag{F5}$$

$$\Delta^{\pm} = \left(\frac{t^2-1}{t} + Y_1^s\right)\left(\frac{t^2-1}{t} + Y_1^b\right) \pm t^{2N}Y_2^sY_2^b, \tag{F6}$$

and the quantities Y_1^a, Y_2^a, Y_1^b, Y_2^b, Y_1^s, and Y_2^s are given by the following expressions:

$$Y_1^a = C_2S_1 + \frac{5}{4}C_1S_2, \tag{F7}$$

$$Y_2^a = C_1S_2 + \frac{5}{4}C_2S_1, \tag{F8}$$

$$Y_1^b = Y_1^s - (C_1S_2 + 2C_2S_1), \tag{F9}$$

$$Y_2^b = Y_2^s - (2S_1 + S_2t), \tag{F10}$$

$$Y_1^s = C_1C_2 + 2S_1S_2 - t, \tag{F11}$$

and

$$Y_2^s = C_1 - C_2t. \tag{F12}$$

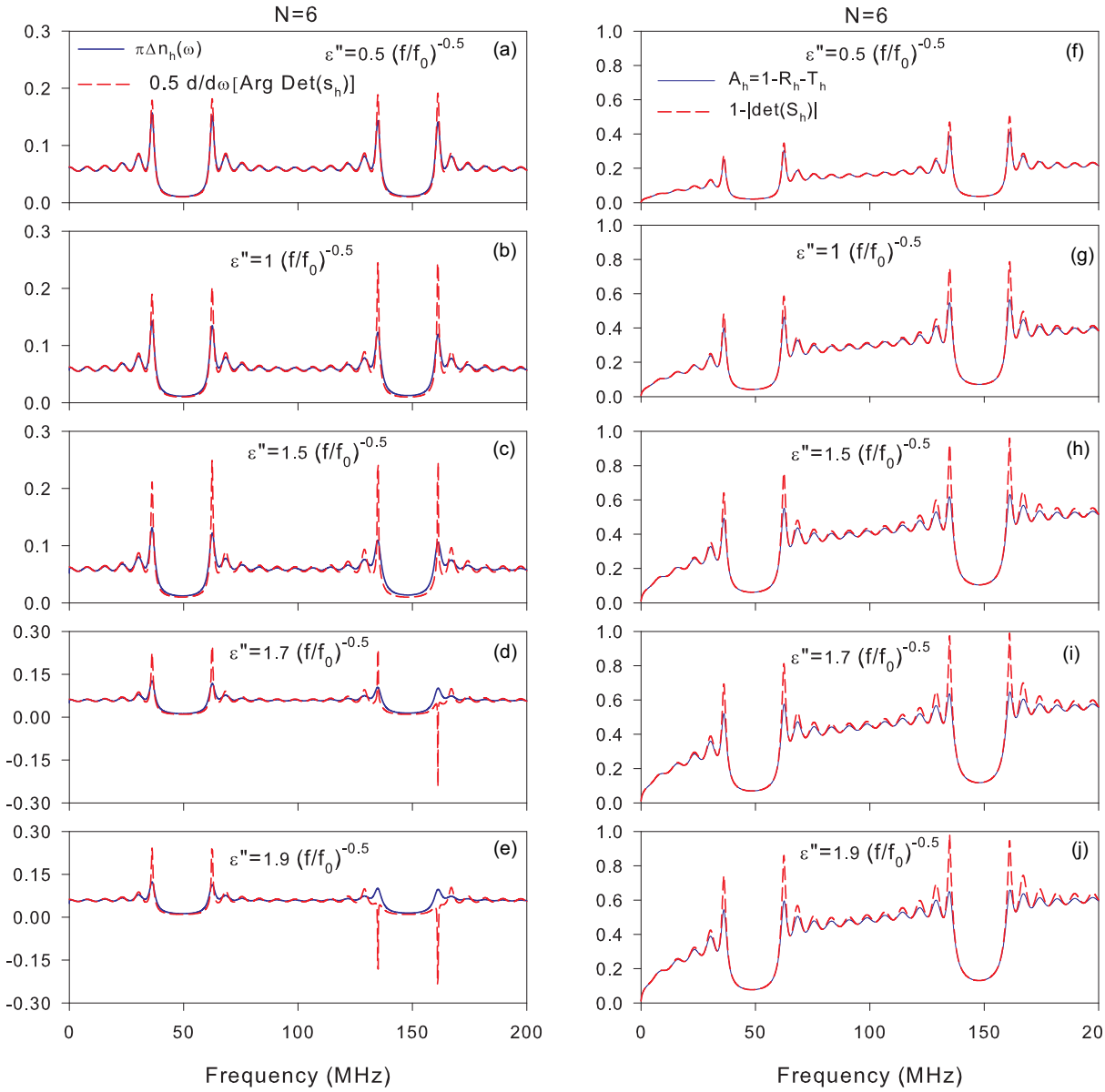

FIG. 13. [(a)–(e)] Theoretical comparison of $\frac{1}{2}\frac{d}{d\omega}\mathrm{Arg}[\det(S_h)]$ and DOS for different values of loss. [(f)–(j)] Theoretical comparison of $A_h = 1 - R_h - T_h$ and $1 - |\det(S_h)|$ for different values of loss. (b) and (g) correspond to the coaxial cable case.

For the vertical system [Fig. 1(d)], the finite structure is grafted vertically along a waveguide. The total DOS can be obtained by the following expression [60]:

$$\Delta n_v(\omega^2) = n_1(\omega^2) + 2n_2(\omega^2) + 2\Delta n_s'(\omega^2), \tag{F13}$$

where

$$\Delta n_s'(\omega^2) = \frac{-\varepsilon}{\pi}\mathrm{Im}\frac{1}{4F}\left\{\frac{1}{4F} + \frac{1}{F}\left[\frac{1}{W}\left(\frac{t^2-1}{t} + Y_1^s\right)(2C_2S_1 + C_1S_2) - t^{2(N-1)}Y_2^s(2S_1 + S_2t)\right]\right\} \tag{F14}$$

and

$$W = \left(\frac{t^2-1}{t} + Y_1^s\right)^2 - \left(t^N Y_2^s\right)^2. \tag{F15}$$

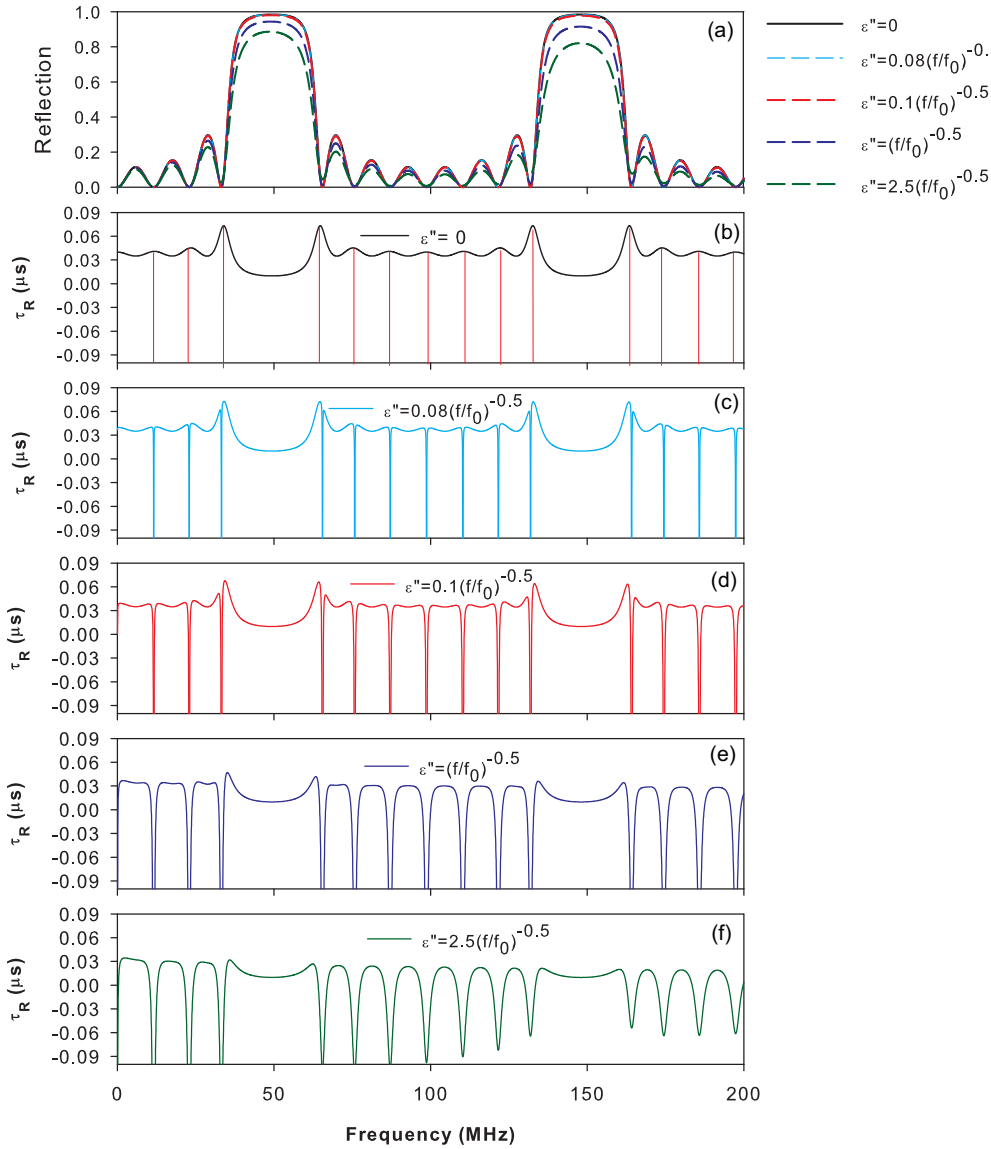

FIG. 14. (a) Reflection amplitude through the finite size system of Fig. 1(b) for different values of loss. [(b)–(f)] Reflection delay time for different values of loss. (e) corresponds to the coaxial cable case.

APPENDIX G: COMPARISON BETWEEN DOS AND $\frac{1}{2}\frac{d}{d\omega}$Arg[(det($S_h$)] AS WELL AS $A_h = 1 - R_h - T_h$ AND $1 - |(\det(S_h)|$ IN PRESENCE OF LOSS

The effect of loss on the relation between DOS and $\frac{1}{2}\frac{d}{d\omega}$Arg[(det($S_h$)] as well as the relation between the absorption and $|(\det(S_h)|$ can be also studied by varying the imaginary part of the permittivity ε''. Figures 13(a)–13(e) give a theoretical comparison between DOS and $\frac{1}{2}\frac{d}{d\omega}$Arg[(det($S_h$)] for $N = 6$ and different values of ε''. For lower values of ε'', we see that the DOS is approximately equivalent to the derivative of the phase of det(S_h) [Fig. 13(a)]. Also, we can notice that the DOS remains almost the same as the derivative of the phase of det(S_h) inside the bands with a noticeable discrepancy between the two spectra at the bulk band edges [Figs. 13(b) and 13(c)]. However, for high values of ε'', the DOS and the derivative of the phase of det(S_h) exhibit different behaviors especially at the band edges where the latter changes sign [Figs. 13(d) and 13(e)]. Indeed, we have checked that det(S_h) vanishes at these frequencies (i.e., $r = \pm t$) and changes sign, giving rise to an abrupt phase change of π in the argument of det(S_h) and therefore a negative delta peak in the derivative of the phase of det(S_h). Figures 13(f)–13(j) give a theoretical comparison between the absorption $A_h = 1 - R_h - T_h$ and $1 - |(\det(S_h)|$ for different values of ε''. We can see a discrepancy between the two latter quantities as far as ε'' increases. In particular, at the band edges when det(S_h) almost vanishes, the absorption becomes simply $A_h = 1 - 2R_h$ (as $R_h = T_h$), whereas $1 - |(\det(S_h)|$ becomes almost unity.

APPENDIX H: COMPARISON BETWEEN DOS AND DELAY TIME IN PRESENCE OF LOSS

In order to show the effect of loss on the relation between the DOS and the reflection delay time in presence of reflection zeros, we have plotted in Fig. 14, the theoretical reflection

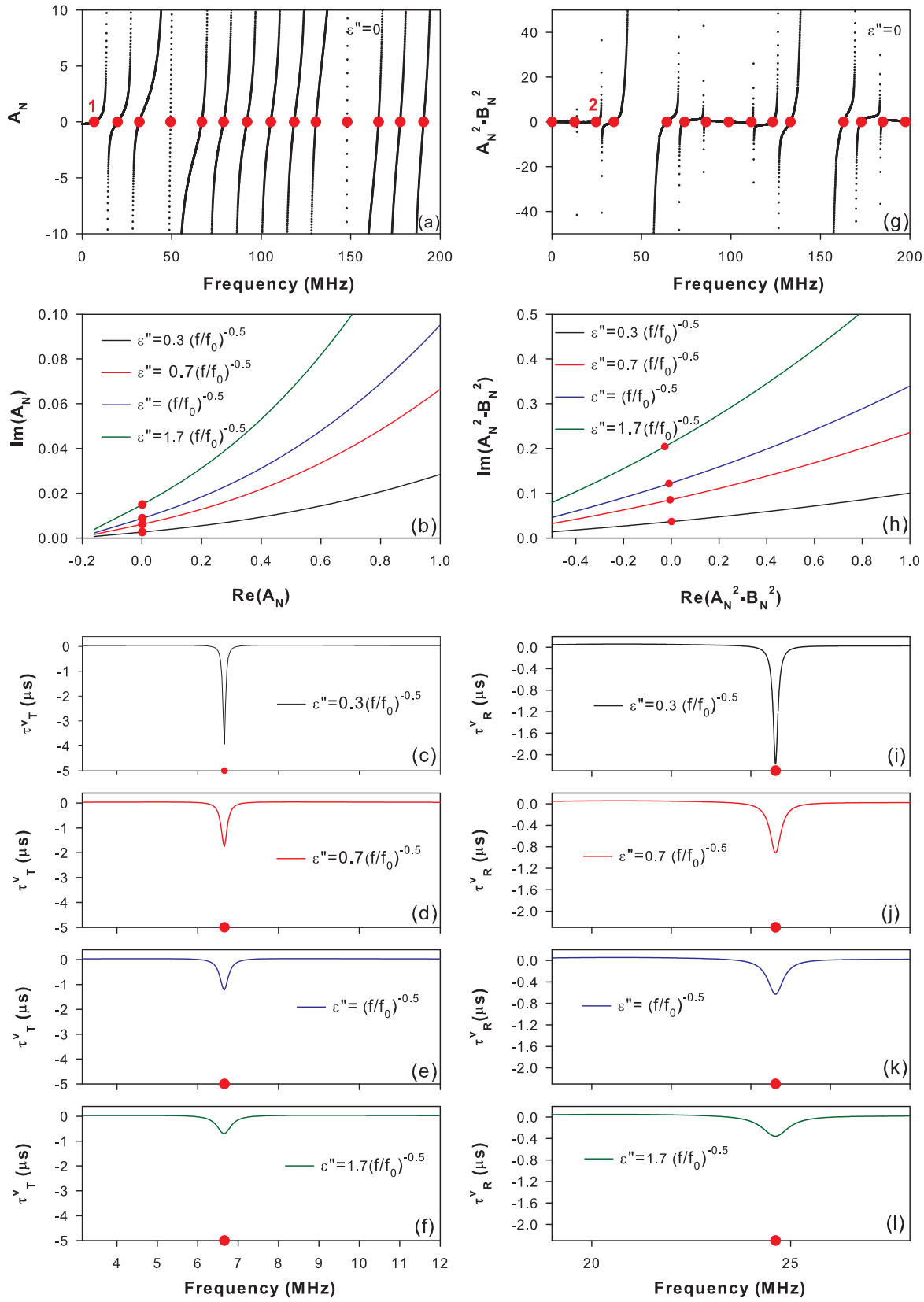

FIG. 15. (a) Variation of A_N as function of frequency for lossless system. Red circles indicate the frequencies for which $A_N = 0$. (b) Real and imaginary parts of A_N around the frequencies associated to the mode labeled 1 in (a). [(c)–(f)] Theoretical transmission delay times for different loss strength. [(g) and (h)] Same as (a), (b) but for $A_N^2 - B_N^2$. [(i)–(l)] Same as (c)–(f) but for the reflection delay time.

coefficient and the corresponding delay times for different values of loss. The blue curves [Fig. 14(e)] correspond to the case of coaxial cables. As mentioned above, for lossless systems the reflection zeros [Fig. 14(a)] give rise to true delta peaks in the delay time indicated by vertical red lines in Fig. 14(b). In this case, apart the delta functions (impossible to observe experimentally) the delay time [black curve in Fig. 14(b)] is equivalent to DOS. For small loss [Fig. 14(c)], the delay spectra still show the shape of the DOS as the negative peaks are now slightly enlarged. For high loss [Figs. 14(d)–14(f)], the delay spectra are quite different from DOS. Similar results are obtained for transmission spectra when the latter present transmission zeros.

APPENDIX I: BEHAVIOR OF A_N AND $A_N^2 - B_N^2$ IN PRESENCE OF LOSS

In absence of loss, all the parameters [A_N (3a), B_N (3b), and $A_N^2 - B_N^2$ (6)] are real quantities, however if loss is taken into account, they become complex. We shall detail below the behaviors of these terms and their meanings with and without loss. In absence of loss, $A_N = 0$ gives the eigenmodes of the system with $H = 0$ boundary condition in one side and $E = 0$ in the other side [Fig. 1(c)]. These modes are indicated by red circles in Fig. 15(a) where A_N vanishes. In presence of loss, the parameter A_N becomes complex. We have presented in Fig. 15(b) its real and imaginary parts around the frequency $f = 6.66$ MHz associated to the mode labeled 1 in Fig. 15(a). We can see that when increasing loss, the real part of A_N remains almost zero, whereas its imaginary part increases slightly. The real part of A_N, responsible of the position of the negative delta peaks (Lorentzians) in Figs. 15(c)–15(f), makes the latter falling at almost the same frequency. However, the imaginary part of A_N, responsible of the width of negative delta peaks in Figs. 15(c)–15(f), makes the latter larger when loss increases.

Similarly, for lossless system the parameter $A_N^2 - B_N^2 = 0$ [Eq. (A27)] gives the eigenmodes of the finite photonic crystal with magnetic wall ($H = 0$) on both sides. Figure 15(g) gives a plot of $A_N^2 - B_N^2$ versus the frequency. The red circles on the abscissa axis give the frequencies of the eigenmodes of such system. These modes coincide with the reflection zeros [see Eq. (28b) and Fig. 10(h)] giving rise to negative delta delay times [Fig. 10(j)]. For a lossy system, $A_N^2 - B_N^2$ becomes a complex. We have presented in Fig. 15(h) its real and imaginary parts around the frequency $f = 24.62$ MHz associated to the mode labeled 2 in Fig. 15(g). The real part of $A_N^2 - B_N^2$ changes very slightly from zero, which does not affect the position of the enlarged negative delta peaks (Lorentzians) in Figs. 15(i)–15(l) below. However, the imaginary part of $A_N^2 - B_N^2$, affects considerably the width of negative delta peaks in Figs. 15(i)–15(l). These results clearly show that even in presence of loss, the frequency positions of the eigenmodes of the finite system are almost unaffected, while the width of these resonances in the delay time enables to detect easily these modes.

[1] C. Kittel, *Introduction to Solid State Physics*, 8th ed. (Wiley, New York, 2004).

[2] S. Datta, *Electronic Transport in Mesoscopic Systems* (Cambridge University Press, Cambridge, 1995).

[3] F. Garcia-Moliner and V. R. Velasco, *Theory of Single and Multiples Interfaces* (World Scientific, Singapore, 1992).

[4] E. N. Economou, *Green's Functions in Quantum Physics* (Springer, Berlin, 2006).

[5] L. Dobrzynski, E. H. El Boudouti, A. Akjouj, Y. Pennec, H. Al-Wahsh, G. Lévêque, and B. Djafari-Rouhani, *Phononics* (Elsevier, Amsterdam, 2017).

[6] J. A. Dobrowolski, *Microwave Network Design Using the Scattering Matrix*, 1st ed. (Artech House, Norwood, Mass, USA, 2010).

[7] M. V. Moskalets, *Scattering Matrix Approach to Non-Stationary Quantum Transport* (Imperial College Press, London, 2012).

[8] J. Tioh, R. J. Weber, and M. Mina, *Magneto-Optical Switches, Optical Switches, Materials and Design*, Woodhead Publishing Series in Electronic and Optical Materials (Woodhead, Philadelphia, 2010), Chap. 4, pp. 97–135.

[9] R. C. Newton, *Scattering Theory of Waves and Particles*, 2nd ed. (Springer-Verlag, New York, 1982).

[10] Y. Avishai and Y. B. Band, Phys. Rev. B **32**, 2674 (1985).

[11] M. Büttiker, J. Phys.: Condens. Matter **5**, 9361 (1993).

[12] V. Gasparian, T. Christen, and M. Büttiker, Phys. Rev. A **54**, 4022 (1996).

[13] M. Brandbyge and M. Tsukada, Phys. Rev. B **57**, R15088 (1998).

[14] S. Souma and A. Suzuki, Phys. Rev. B **65**, 115307 (2002).

[15] J. Ruiz, E. Jüdar, and V. Gasparian, Phys. Rev. B **75**, 235123 (2007).

[16] V. Vargiamidis and V. Fessatidis, Phys. Lett. A **374**, 4438 (2010).

[17] J. Friedel, Philos. Mag. **43**, 153 (1952).

[18] T. Taniguchi and M. Büttiker, Phys. Rev. B **60**, 13814 (1999).

[19] H. W. Lee, Phys. Rev. Lett. **82**, 2358 (1999).

[20] A. Yacoby, M. Heiblum, D. Mahalu, and H. Shtrikman, Phys. Rev. Lett. **74**, 4047 (1995).

[21] R. Schuster, E. Buks, M. Heiblum, D. Mahalu, V. Umansky, and H. Shtrikman, Nature (London) **385**, 417 (1997).

[22] Y. Imry, *Introduction to Mesoscopic Physics* (Oxford University Press, New York, 1997).

[23] L. A. MacColl, Phys. Rev. **40**, 621 (1932).

[24] H. G. Winful, Phys. Rep. **436**, 1 (2006).

[25] Ph. Balcou and L. Dutriaux, Phys. Rev. Lett. **78**, 851 (1997).

[26] M. Deutsch and J. E. Golub, Phys. Rev. A **53**, 434 (1996).

[27] A. M. Steinberg, P. G. Kwiat, and R. Y. Chiao, Phys. Rev. Lett. **71**, 708 (1993).

[28] Ch. Spielmann, R. Szipöcs, A. Stingl, and F. Krausz, Phys. Rev. Lett. **73**, 2308 (1994).

[29] P. Pereyra, Phys. Rev. Lett. **84**, 1772 (2000).

[30] N. Ouchani, A. El Moussaouy, H. Aynaou, Y. El Hassouani, E. H. El Boudouti, and B. Djafari-Rouhani, J. Appl. Phys. **122**, 183106 (2017).

[31] N. Opačak, V. Milanović, and J. Radovanović, Opt. Quant. Electron **50**, 142 (2018).

[32] A. Ranfagni, D. Mugnai, P. Fabeni, and G. P. Pazzi, Appl. Phys. Lett. **58**, 774 (1991).

[33] A. Enders and G. Nimtz, Phys. Rev. B **47**, 9605 (1993).

[34] H.-Y. Yao, N. C. Chen, T.-H. Chang, and H. G. Winful, IEEE Trans. Microw. Theory Techn. **64**, 3121 (2016).

[35] Y. Yang and M. Sumetsky, Opt. Lett. **45**, 762 (2020).

[36] D. B. Stojanović, J. Radovanović, and V. Milanović, Phys. Rev. A **94**, 023848 (2016).

[37] M. Asano, K. Y. Bliokh, Y. P. Bliokh, A. G. Kofman, R. Ikuta, T. Yamamoto, Y. S. Kivshar, L. Yang, N. Imoto, S. K. Özdemir, and F. Nori, Nat. Communc. **7**, 13488 (2016).

[38] M. M. Sanchez-Lopez, A. Sanchez-Merono, J. Arias, J. A. Davis, and I. Moreno, Appl. Phys. Lett. **93**, 074102 (2008).

[39] J. Arias, A. Sanchez-Merono, M. M. Sanchez-Lopez, and I. Moreno, Phys. Rev. A **85**, 033815 (2012).

[40] A. Haché and L. Poirier, Phys. Rev. E **65**, 036608 (2002).

[41] J. N. Munday and W. M. Robertson, Appl. Phys. Lett. **81**, 2127 (2002).

[42] E. H. El Boudouti, N. Fettouhi, A. Akjouj, B. Djafari-Rouhani, A. Mir, J. O. Vasseur, L. Dobrzynski, and J. Zemmouri, J. Appl. Phys. **95**, 1102 (2004).

[43] R. S. Anwar, L. Mao, and H. Ning, Appl. Sci. **8**, 1689 (2018).

[44] J. M. Bendickson, J. P. Dowling, and M. Scalora, Phys. Rev. E **53**, 4107 (1996).

[45] M. L. H. Lahlaouti, A. Akjouj, B. Djafari-Rouhani, L. Dobrzynski, M. Hammouchi, E. H. El Boudouti, A. Nougaoui, and B. Kharbouch, Phys. Rev. B **63**, 035312 (2001).

[46] S. Prasad, Y. Sharma, S. Shukla, and V. Singh, Phys. Plasmas **23**, 032123 (2016).

[47] X. Wang, H. Wang, and F. Zheng, Opt. Communic. **382**, 371 (2017).

[48] C. Hess, in *Introduction to Scanning Tunneling Spectroscopy of Correlated Materials*, edited by Eva Pavarim, E. Koch, J. Van den Brink, and G. Swatzky, Quantum Materials: Experiments and Theory (Forschungszentrum Jülich, Germany, 2016).

[49] D. Neumaier, M. Turek, U. Wurstbauer, A. Vogl, M. Utz, W. Wegscheider, and D. Weiss, Phys. Rev. Lett. **103**, 087203 (2009).

[50] W. Sturhahn, T. S. Toellner, E. E. Alp, X. Zhang, M. Ando, Y. Yoda, S. Kikuta, M. Seto, C. W. Kimball, and B. Dabrowski, Phys. Rev. Lett. **74**, 3832 (1995).

[51] A. Mouadili, E. H. El Boudouti, A. Soltani, A. Talbi, A. Akjouj, and B. Djafari-Rouhani, J. Appl. Phys. **113**, 164101 (2013).

[52] A. Mouadili, E. H. El Boudouti, A. Soltani, A. Talbi, B. Djafari-Rouhani, A. Akjouj, and K. Haddadi, J. Phys.: Condens. Matter **26**, 505901 (2014).

[53] J. O. Vasseur, A. Akjouj, L. Dobrzynski, B. Djafari- Rouhani, and E. H. El Boudouti, Surf. Sci. Rep. **54**, 1 (2004).

[54] E. H. El Boudouti, Y. El Hassouani, B. Djafari-Rouhani, and H. Aynaou, Phys. Rev. E **76**, 026607 (2007).

[55] G. J. Schneider, S. Hanna, J. L. Davis, and G. H. Watson, J. Appl. Phys. **90**, 2642 (2001).

[56] Z. Q. Zhang, C. C. Wong, K. K. Fung, Y. L. Ho, W. L. Chan, S. C. Kan, T. L. Chan, and N. Cheung, Phys. Rev. Lett. **81**, 5540 (1998).

[57] H. Aynaou, E. H. El Boudouti, Y. El Hassouani, A. Akjouj, B. Djafari-Rouhani, J. Vasseur, A. Benomar, and V. R. Velasco, Phys. Rev. E **72**, 056601 (2005).

[58] Y. El Hassouani, H. Aynaou, E. H. El Boudouti, B. Djafari-Rouhani, A. Akjouj, and V. R. Velasco, Phys. Rev. B **74**, 035314 (2006).

[59] M. L. H. Lahlaouti, A. Akjouj, B. Djafari-Rouhani, L. Dobrzynski, M. Hammouchi, E. H. El Boudouti, and A. Nougaoui, J. Opt. Soc. Am. A **16**, 1703 (1999).

[60] B. Djafari-Rouhani and L. Dobrzynski, J. Phys.: Condens. Matter **5**, 8177 (1993).

[61] C. Texier, J. Phys. A: Math. Gen. **35**, 3389 (2002).

[62] A. Merkel, G. Theocharis, O. Richoux, V. RomeroGarcia, and V. Pagneux, Appl. Phys. Lett. **107**, 244102 (2015).

[63] N. W. Ashcroft and N. D. Mermin, *Solid State Physics* (Brooks Colle, New York, 1976).

[64] A. Sanchez-Merono, J. Arias, and M. Sanchez-Lopez, IEEE J. Quantum Electron. **46**, 546 (2010).

[65] A. Akjouj, H. Al-Wahsh, B. Sylla, B. Djafari-Rouhani, and L. Dobrzynski, J. Phys.: Condens. Matter **16**, 37 (2004).

[66] T. Mrabti, Z. Labdouti, A. Mouadili, E. H. El Boudouti, B. Djafari-Rouhani, Physica E **116**, 113770 (2020).

[67] H. Al-Wahsh, A. Akjouj, B. Djafari-Rouhani, and L. Dobrzynski, Surf. Sci. Rep. **66**, 29 (2011).

[68] L. Dobrzynski, Surf. Sci. Rep. **11**, 139 (1990).

[69] L. Dobrzynski, J. Mendialdua, A. Rodriguez, S. Bolibo, and M. More, J. Phys. (France) **50**, 2563 (1989).

[70] M. L. Bah, A. Akjouj, and L Dobrzynski, Surf. Sci. Rep. **16**, 97 (1992).

[71] E. H. El Boudouti, B. Djafari-Rouhani, E. M. Khourdifi, and L. Dobrzynski, Phys. Rev. B **48**, 10987 (1993).

[72] D. S. Fisher and P. A. Lee, Phys. Rev. B **23**, 6851 (1981).